

## FORMATION OF GLOBULAR CLUSTERS IN HIERARCHICAL COSMOLOGY

Andrey V. Kravtsov

Department of Astronomy and Astrophysics and Center for Cosmological Physics

The University of Chicago, Chicago, IL 60637

andrey@oddjob.uchicago.edu

Oleg Y. Gnedin

Space Telescope Science Institute

3700 San Martin Drive, Baltimore, MD 21218

ognedin@stsci.edu

Draft version February 7, 2020

## ABSTRACT

We study the formation of globular clusters in a Milky Way-size galaxy using a high-resolution cosmological simulation. The clusters in our model form in the strongly baryon-dominated cores of supergiant molecular clouds in the gaseous disks of high-redshift galaxies. The properties of clusters are estimated using a physically-motivated subgrid model of the isothermal cloud collapse. The first clusters in the simulation form at  $z = 12$ , while the best conditions for globular cluster formation appear to be at  $z = 3-5$ . Most clusters form in the progenitor galaxies of the virial mass  $M_h > 10^9 M_\odot$  and the total mass of the cluster population is strongly correlated with the mass of its host galaxy:  $M_{GC} = 3.2 \cdot 10^6 M_\odot (M_h = 10^{11} M_\odot)^{1.13 \pm 0.08}$ . This corresponds to a fraction  $2-10^{-4}$  of the galactic baryons being in the form of globular clusters. In addition, the mass of the globular cluster population and the maximum cluster mass in a given region strongly correlates with the local average star formation rate. We find that the mass, size, and metallicity distributions of the globular cluster population identified in the simulation are remarkably similar to the corresponding distributions of the Milky Way globulars. We find no clear mass-metallicity or age-metallicity correlations for the old clusters. The zero-age mass function of globular clusters can be approximated by a power-law  $dN = dM / M^\alpha$  with  $\alpha = 2$ , in agreement with the mass function of young stellar clusters in starbursting galaxies. However, the shape of the zero-age mass function may be better described by the high-mass tail of a log-normal distribution which peaks at  $\sim 10^3 M_\odot$ . In particular, the logarithmic slope of the mass function in the model steepens with increasing mass, suggesting the possible existence of a maximum cluster mass. We discuss in detail the origin, universality, and dynamical evolution of the globular cluster mass function. Our results indicate that globular clusters with properties similar to those of observed clusters can form naturally within young dense gaseous disks at  $z \approx 3$  in the concordance CDM cosmology.

Subject headings: cosmology: theory {galaxies: formation {globular clusters: formation {methods: numerical}

## 1. introduction

More than seventy years ago in a monograph entitled *Star Clusters* Harlow Shapley (1930) wrote: 'It is encouraging to see how fragile and futile are the majority of astronomical theories and speculations... for the futility of speculations emphasizes the importance and durability of observations and indicates the steady progress of the science.' These words are particularly true for the models of globular cluster (GC) formation. Extensive observational surveys of globular cluster systems in the Milky Way and other galaxies have been compiled during the past two decades (e.g., Harris 2001). At the same time, despite a wide variety of proposed models, a self-consistent scenario of globular cluster formation is yet to be constructed.

The existing models can be classified into four broad categories. In the primary models globular clusters are envisioned to have formed soon after recombination, with masses determined by the cosmological Jeans mass (Peebles & Dicke 1968; Peebles 1984). In the secondary models, globular clusters are assumed to appear during the early stages of galaxy formation. For instance, Fall & Rees (1985) pointed out that thermal instability in hot gaseous halos of young galaxies can naturally lead to the condensation of globular cluster-size clouds. Several other trigger

mechanisms operating during galaxy formation, such as the shock compression and collisions of primordial molecular clouds, were also explored (Gunn 1980; Burkert et al. 1992; Murray & Lin 1992; Larson 1996; Harris & Pudritz 1994; Cen 2001).

Models of the third class correspond to the relatively recent stages of galaxy formation. Schweizer (1987) and Ashman & Zepf (1992), for example, proposed a model of GC formation in the gas-rich mergers of disk galaxies. These mergers perturb, compress, and shock the interstellar medium which creates the very high pressure regions conducive to GC formation. Accordingly, this model predicted that young clusters should be present in merging and interacting galaxies. These predictions were successfully confirmed by HST observations (Whitmore & Schweizer 1995; Holtzman et al. 1996; Whitmore et al. 1999; Zepf et al. 1999).

The division between the second and third classes of models is somewhat blurred. In the current hierarchical structure formation paradigm, galaxy formation is a continuous process of merging and accretion. The fourth, most recent class of models thus incorporates the elements of all previous classes within the hierarchical framework (Cote et al. 2000, 2002; Beasley et al. 2002; Gnedin 2003). Globular clusters in these models are assumed to form

in young disks which undergo frequent mergers. At this point, the models are largely phenomenological and characterize the cluster formation using somewhat ad hoc recipes, limiting their predictive power. Nevertheless, they have been fairly successful in reproducing many properties of the observed GC populations. The comparisons of various models to observations can be found in Harris (2001) and Gnedin et al. (2001).

The main obstacle to building a realistic and self-consistent physical model of globular cluster formation has always been the uncertainty in the initial conditions. In fact, all of the models mentioned above would produce star clusters in environments where the conditions agree with the model assumptions. Another unknown is the connection between globular clusters and galaxies. On the one hand, the largest globular clusters have masses comparable to those of dwarf spheroidal galaxies ( $10^7 M_{\odot}$ ). On the other, globular clusters do not seem to have extended dark matter halos (e.g., Moore 1996) and in that respect differ fundamentally from galaxies. There is also significant disparity between the densities, velocity dispersions, and structural parameters of dwarf galaxies and globular clusters (Kormendy 1985). In order to understand these differences we need a self-consistent model which ties the formation of globular clusters to the realistic formation and evolution of their parent galaxies.

The theory of hierarchical galaxy formation has matured in the last decade, motivated by the theory of inflation, guided by observations, and aided by elaborate numerical simulations. In hierarchical models, galaxies form via gravitational instability from small-amplitude initial Gaussian fluctuations with well-defined statistical properties. Recently, this scenario has been spectacularly confirmed by the CMB anisotropy measurements and other cosmological probes (e.g., Spergel et al. 2003). The spatially flat cosmological model dominated by the dark energy and cold dark matter (CDM) favored by observations provides a solid framework for the theory of globular cluster formation.

Cosmological simulations follow the hierarchical build-up of galaxies self-consistently within a given model starting from the well-defined initial conditions. These simulations are now reaching the level of sophistication and dynamical range sufficient to study the formation and dynamics of giant molecular clouds in galactic disks. Therefore, we can address the formation of the proto-cluster clouds without resorting to phenomenological parameterization and directly study the details of when, where, and how globular clusters formed.

The main goal of this work is to study the formation of globular cluster populations in the hierarchical scenario using a very high-resolution cosmological simulation of galaxy formation. Based on observational evidence, we assume that clusters form in dense isothermal cores of the super giant molecular clouds ubiquitous in high-redshift galactic disks. In addition, we use a simple model of isothermal collapse to derive the properties of stellar clusters that would form in each core. We then compare the derived properties of model globular clusters with those of the GC population in the Galaxy as well as with the populations of young GCs in external galaxies.

Many decades ago, Harlow Shapley used the distribution

of globular clusters to greatly expand and refine the structure of our Galaxy. It is only fitting that we now apply our understanding of galaxy formation to predict and explain the properties of globular clusters.

## 2. numerical simulations

### 2.1. Numerical techniques and Physical Processes

The simulations presented in this paper were performed using the Eulerian gasdynamical N-body Adaptive Remesh Tree (ART) code. This code is based on the cell-based approach to adaptive mesh refinement (AMR) developed by Khokhlov (1998). The algorithm uses a combination of multi-level particle-mesh (Krivtsov et al. 1997; Kravtsov 1999) and shock-capturing Eulerian methods (van Leer 1979; Colella & Glaz 1985) to follow the evolution of dark matter (DM) and gas, respectively. High dynamical range is achieved by applying adaptive mesh refinement both to the gasdynamics and gravity calculations.

Several physical processes critical to various aspects of galaxy formation are implemented in this code: star formation; metal enrichment and thermal feedback due to the supernovae type II and type Ia (SN II/Ia); self-consistent advection of metals; metallicity- and density-dependent cooling and UV heating due to the cosmological ionizing background, using the cooling and heating rates tabulated in the temperature range  $10^2 < T < 10^9$  K for a grid of densities, metallicities, and UV intensities using Cloudy (ver. 96b4, Ferland et al. 1998). In the present simulations we set a minimum temperature of  $T_{\text{min}} = 300$  K. The cooling and heating rates take into account Compton heating/cooling of plasma, UV heating, atomic and molecular cooling. While the detailed implementation of these processes is described elsewhere (Krivtsov 2003a,b), below we summarize the details crucial to this study.

We use a "constant efficiency" star formation prescription. Namely, the stars are formed with a constant timescale so that the star formation rate is proportional to the local gas density,  $\dot{m} / \rho$ . This prescription is motivated by observations of the star forming regions (e.g., Young et al. 1996; Wong & Blitz 2002) and appears to reproduce the Schmidt-like law of star formation on kpc scales (Krivtsov 2003b). Star formation was allowed to take place only in the coldest and densest regions,  $T < T_{\text{SF}}$  and  $\rho > \rho_{\text{SF}}$ , but no other criteria (like the collapse condition  $\nabla \cdot \mathbf{v} < 0$ ) were imposed. We used  $T_{\text{SF}} = 4$  G yrs,  $\rho_{\text{SF}} = 9000$  K, and  $\rho_{\text{SF}} = 1.64 M_{\odot} \text{ pc}^{-3}$  or the atomic hydrogen number density of  $n_{\text{H}} = 50 \text{ cm}^{-3}$ . The adopted values of  $T_{\text{SF}}$  and  $\rho_{\text{SF}}$  are quite different from the typical temperatures and densities of star forming molecular cores:  $T = 30 - 50$  K and  $n_{\text{H}} = 10^4 \text{ cm}^{-3}$ . They are, however, more appropriate for the identification of star forming regions on 100 pc scales which are resolved in the presented simulations. In practice,  $T_{\text{SF}}$  is not relevant because most of the gas with  $\rho > \rho_{\text{SF}}$  is at temperatures of just a few hundred degrees Kelvin.

Each newly formed stellar particle is treated as a single-age stellar population and its feedback on the surrounding gas is implemented accordingly. The word feedback is used here in a broad sense to include the injection of energy and heavy elements (metals) via stellar winds and supernovae, and the secular stellar mass loss. Specifically, we assume that the stellar initial mass function (IMF) is

described by the Miller & Scalo (1979) functional form with stellar masses in the range  $0.1 - 100 M_{\odot}$ . All stars with  $m > 8 M_{\odot}$  deposit  $2 \times 10^{51}$  ergs of thermal energy and a mass  $f_{\text{Z}} m$  of heavy elements in their parent cell (no delay of cooling is introduced in these cells). The metal fraction is  $f_{\text{Z}} = m \text{ in } (0.2; 0.01m - 0.06)$ , which crudely approximates the results of Woosley & Weaver (1995). In addition, the stellar particles return a fraction of their mass and metals to the surrounding gas at a secular rate  $\dot{m}_{\text{loss}} = m \cdot C_0 (t - t_{\text{birth}} + T_0)^{-1}$  with  $C_0 = 0.05$  and  $T_0 = 5 \text{ Myr}$  (Jungwiert et al. 2001). The released metals are advected along with the gas. The code also accounts for SN Ia feedback assuming a rate that slowly increases with time and broadly peaks at the population age of 1 Gyr. We assume that the fraction  $5 \times 10^{-3}$  of mass in stars between 3 and  $8 M_{\odot}$  explodes as SN Ia over the entire population history and each SN Ia dumps  $2 \times 10^{51}$  ergs of thermal energy and ejects  $1.3 M_{\odot}$  of metals into parent cell. For the assumed IMF, 75 SN II (instantly) and 11 SN Ia (over several billion years) are produced by a  $10^4 M_{\odot}$  stellar population.

## 2.2. Simulation Parameters

The simulation we use in our analysis follows the early ( $z = 3$ ) stages of evolution for a galaxy of typical mass:  $10^{12} h^{-1} M_{\odot}$  at  $z = 0$ . At the analyzed epochs, the galaxy has already built up a significant portion of its total mass:  $1.3 \times 10^{10} h^{-1} M_{\odot}$  at  $z = 9$  and  $2 \times 10^{11} h^{-1} M_{\odot}$  at  $z = 4$ . The total galaxy mass,  $M_h$ , is defined as the mass enclosed within the radius of the average density equal 340 times the mean matter density. The simulation starts from a random realization of the Gaussian density field at  $z = 50$  in a periodic box of  $6 h^{-1} \text{ comoving Mpc}$  with the power spectrum (Hu & Sugiyama 1996) appropriate to the CDM model:  $\sigma_8 = 1$ ,  $n_s = 0.3$ ,  $b = 0.043$ ,  $h = H_0/100 = 0.7$ ,  $n_s = 1$ , and  $\sigma_8 = 0.9$ . The parameters have their usual meaning and are consistent with recent cosmological constraints (e.g., Spergel et al. 2003).

To increase mass resolution, a low resolution simulation was run first and a galactic-mass halo was selected. A lagrangian region corresponding to five virial radii of the object at  $z = 0$  was then identified at  $z = 50$  and resampled with additional small-scale waves (Klypin et al. 2001). The total number of DM particles in the high-resolution lagrangian region is  $2.64 \times 10^6$  and each particle mass is  $m_{\text{DM}} = 9.18 \times 10^5 h^{-1} M_{\odot}$ . Outside the high-resolution region the matter distribution was sampled with  $3 \times 10^5$  higher mass particles.

As the matter distribution evolves, the code adaptively and recursively refines the mesh in the high density regions. Initially, a uniform  $64^3$  grid covered the entire computational box. The lagrangian region, however, was always unconditionally refined to the third refinement level, corresponding to an effective grid size of  $512^3$ . Beyond the third level, a mesh cell was tagged for refinement if its gas or DM mass exceeded 0.125 and 0.0625 times the mean mass expected for the average density in each component in the zeroth level (i.e., uniform grid) cell, respectively. The refinement thus follows the collapse of  $1.2 \times 10^6 h^{-1} M_{\odot}$  (gas) and  $3.7 \times 10^6 h^{-1} M_{\odot}$  (DM) mass elements in a quasi-lagrangian fashion.

The maximum allowed refinement level  $l_{\text{max}}$  was set to

nine. A total of  $1.1 \times 10^7$  mesh cells was used at  $z = 4$  with  $2.5 \times 10^5$  of them at refinement levels of 8 and 9. The high-density cold star forming disks within DM halos were refined to  $l_{\text{max}} = 9$ . The physical size of mesh cells was  $x_1 = 26.16 [10 = (1 + z)]^{2^{-1}} \text{ pc}$ , where  $l$  is the cell's level of refinement. Each refinement level was integrated with its own time step  $t_1 = t_0 2^{-1} \times 2 \times 10^4 2^{9-1} \text{ yrs}$ , where  $t_0 = 10^7 \text{ yrs}$  is the global time step on the zeroth level set using the Courant-Friedrichs-Levy condition.

## 2.3. Identification of the Globular Cluster Formation Sites

Although the resolution achieved in the simulation is very high in the disk region, it is clearly insufficient to resolve the formation of stellar clusters. The resolution, however, is sufficient to identify the potential sites for GC formation. The cores of giant molecular clouds in high-redshift galaxies are the natural candidates (Harris & Pudritz 1994; McLaughlin & Pudritz 1996) for such sites. Numerical simulations of Nakasato et al. (2000) show that globular clusters with realistic masses and sizes can indeed form in such cores. We therefore adopt this picture and identify the cores of dense gaseous clouds in simulated disks as the sites of globular cluster formation.

We identify giant molecular clouds using the following algorithm. All mesh cells with gas densities greater than a certain threshold density,  $\rho_{\text{th}}$ , are selected and sorted into a list of increasing density. The highest density cell and all of its immediate neighbors are then included in the first cloud. This cell is labeled as the core cell of the cloud. The next highest density cell in the list is then considered. If it happens to be already included in the first cloud, all of its immediate neighbor cells are then also included in the first cloud. If, on the other hand, the cell is not part of a cloud yet, it is assigned to a new cloud and is labeled as its core. The procedure repeats until the list of cells is exhausted. The algorithm is thus somewhat similar, but not equivalent, to the well-known friends-of-friends clustering algorithm. The current implementation will break a region into separate clouds for each density peak rather than combining several peaks into the same cloud.

We explored several values of the threshold density  $\rho_{\text{th}} = 1 - 50 M_{\odot} \text{ pc}^{-3}$  for the cloud identification. Although the cloud masses grow and ever smaller clouds are included in the catalog as the threshold is decreased, in the mass range relevant for the GC identification the same cores are identified for different  $\rho_{\text{th}}$ . For our analysis below we choose the cloud catalog with the fiducial value  $\rho_{\text{th}} = 1 M_{\odot} \text{ pc}^{-3}$ . This corresponds to the gas number density  $40 \text{ cm}^{-3}$  and pressure  $\approx 10^4 \text{ K cm}^{-3}$ . Note that at these densities the gas temperature is at the lowest value allowed in the simulation:  $T_{\text{min}} = 300 \text{ K}$ .

## 2.4. The Subgrid Model

In order to derive the properties of star clusters forming in molecular cloud cores, we complement the simulations with a physical description of the gas distribution on a subgrid level. Observations of star forming regions in the solar neighborhood (e.g., Elmegreen 2002) show that clustered star formation proceeds inevitably when the cores of molecular clouds reach a critical density  $\approx 10^5 \text{ cm}^{-3}$ .

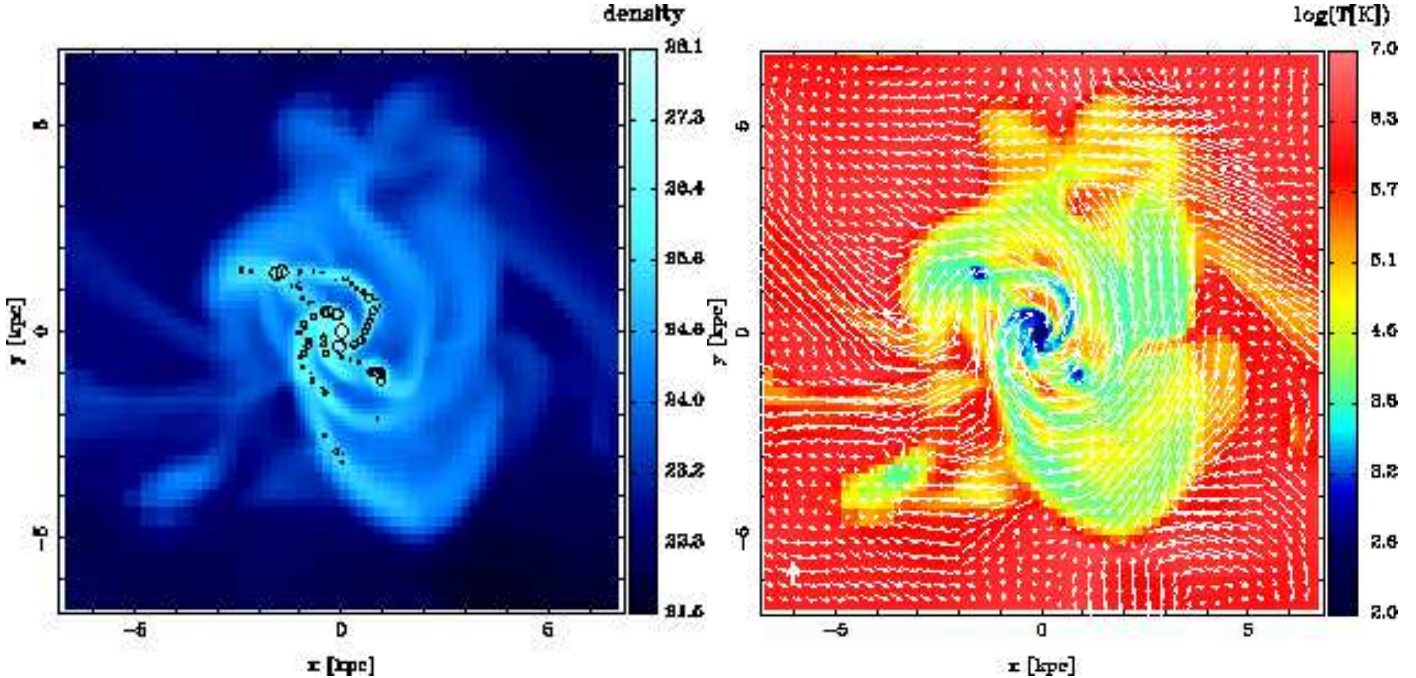


Fig. 1. Gas density (left panel) and temperature (right panel) in the most massive disk at  $z = 4$ . The projected density is in  $\text{cm}^{-2}$ , while the density-weighted average temperature is in degrees Kelvin. The vectors in the right panel show gas velocities; the thick vertical vector in the lower-left corner of the panel corresponds to  $200 \text{ km s}^{-1}$ . The density and temperature are projected over a 3.5 kpc slice centered on the cell of the maximum gas density (the center of the plot). The figure shows a nearly face-on disk with prominent spiral arms in the process of very active accretion and merging. In our model the globular clusters form in the densest regions of the disk corresponding to the darkest knots in the temperature map. The globular clusters identified in the disk at this epoch are shown by circles in the left panel. The radius of the circles corresponds to the mass of each cluster.

Formation of young massive clusters is also accompanied by a high external pressure,  $P_{\text{ext}} > 10^7 \text{ K cm}^{-3}$ . Within such cores, star clusters form with a locally-high efficiency (Kroupa et al. 2001; Geyer & Burkert 2001):

$$\frac{M_{\text{stars}}}{M_g} \approx 0.5; \quad (1)$$

which is also required in order to produce gravitationally-bound clusters. On the theoretical side, analytical models and numerical simulations also indicate that dense bound clusters can form quickly and efficiently in the cores of giant molecular clouds of moderate metallicity (e.g., Harris & Pudritz 1994; McLaughlin & Pudritz 1996; Nakasato et al. 2000). In the models of molecular clouds including thermal support, turbulence, and magnetic fields star formation proceeds rapidly, on one or two dynamical times (Pringle 1989; Ostriker et al. 2001; Bate et al. 2003).

Based on these observational and theoretical results, we implement the following phenomenological subgrid model. At high densities in the smallest cells the cooling time ( $t_{\text{cool}} = 6.6 \cdot 10^5 n^{-1} T_4^{-1} \text{ yr} = 25 \text{ yr}$ ) is much shorter than the dynamical time ( $t_{\text{dyn}} = 5.2 \cdot 10^7 n^{-1/2} \text{ yr}$ ), and we can assume an isothermal structure of the unresolved cloud. The isothermal structure is also seen in the numerical simulations of the collapse of cloud cores by Nakasato et al. (2000). The average density within  $r$  is then  $\rho_{\text{av}}(r) = 3 g(r)$ , while the cell density measured in the simulation is  $\rho_{\text{cell}} = \rho_{\text{av}}(R_{\text{cell}})$ , and the inner density profile is

$$g(r < R_{\text{cell}}) = \frac{1}{3} \frac{r^2}{R_{\text{cell}}} : \quad (2)$$

We assume that a single cluster forms within the cloud core on a dynamical time at the densities and

pressures higher than the critical,  $\rho_{\text{sf}}$ . The radius of the core  $R_{\text{sf}}$  is determined by the condition  $\rho_g(R_{\text{sf}}) = \rho_{\text{sf}}$ . All gas within  $R_{\text{sf}}$  is converted into stars with the efficiency  $\eta : M = M_g(R_{\text{sf}})$ . As a result of gradual loss of the remaining gas, the star cluster expands almost adiabatically (Geyer & Burkert 2001) such that its final size is  $R = R_{\text{sf}} = \eta$ . The resulting average density of the clusters is

$$\rho_{\text{gc}} = \frac{M}{(4/3)\pi R^3} = \frac{4 M_g(R_{\text{sf}})}{(4/3)\pi R_{\text{sf}}^3} = 3^4 \rho_{\text{sf}} : \quad (3)$$

We use the fiducial values  $\eta = 0.6$  and  $\rho_{\text{sf}} = 10^4 M_{\odot} \text{ pc}^{-3}$ , which gives  $\rho_{\text{gc}} = 4 \cdot 10^3 M_{\odot} \text{ pc}^{-3}$ . For the cells of the maximum level of refinement ( $l = 9$ ) the cluster sizes and masses scale as

$$R = \frac{1.3}{1+z} \frac{\text{cell}}{1 M_{\odot} \text{ pc}^{-3}} \text{ pc} ; \quad (4)$$

$$M = \frac{3.3 \cdot 10^4}{(1+z)^3} \frac{\text{cell}}{1 M_{\odot} \text{ pc}^{-3}} M_{\odot} : \quad (5)$$

The fiducial parameters match the observed properties of the Milky Way globular clusters. The median density at the half-mass radius for the whole Galactic sample is  $3 \cdot 10^3 M_{\odot} \text{ pc}^{-3}$ , while for the clusters less affected by dynamical evolution ( $M > 10^5 M_{\odot}$ ) it is  $7 \cdot 10^3 M_{\odot} \text{ pc}^{-3}$ . The properties of the model clusters in the simulation fall right in the middle of this range.

Note that the mass function of globular clusters at birth will be significantly modified by the effects of dynamical evolution. As we show in x6, low-mass and low-density clusters are preferentially dissolved by the combined effects

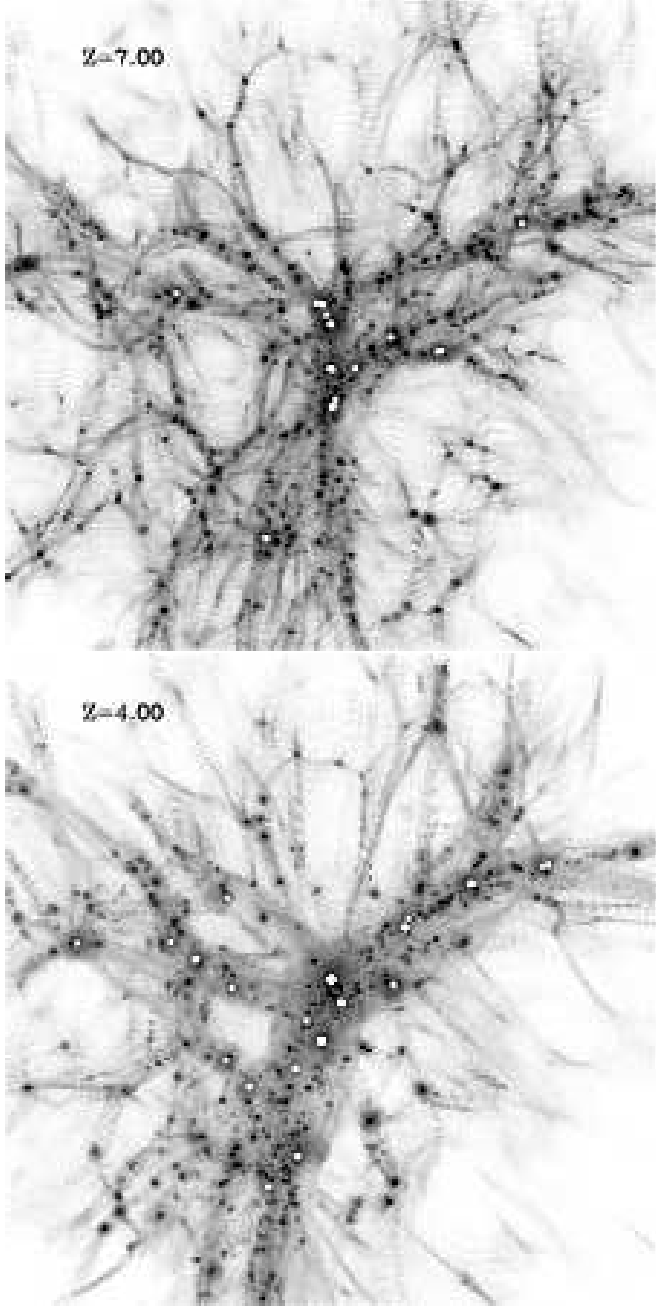


Fig. 2. The identified globular clusters within the global distribution of dark matter at  $z = 7$  and  $z = 4$ . The view is centered on the largest galaxy in the simulation and shows  $1h^{-1} Mpc$  region (comoving). The gray-scale colored particles represent the dark matter, while white circles in the centers of some halos show locations of the globular clusters identified in the simulation. Note that massive halos contain multiple clusters in their centers. The dark matter particles are colored according to the local density on a logarithmic stretch.

of two-body relaxation, tidal shocking, dynamical friction, and stellar evolution. High-mass clusters, on the other hand, preserve their mass function and trace the initial distribution (e.g., Fall & Zhang 2001; Gnedin 2003).

### 3. results

We analyze the simulation outputs at twelve epochs between redshifts  $z = 11.8$  and  $3.35$ , identifying the cores of the giant molecular clouds and computing properties

of the model globular clusters, as described in § 2.3 and 2.4. The time intervals between the outputs are in the range  $100 - 300$  M yrs. Due to limited computational resources, the simulation was run only until  $z = 3.3$ .

#### 3.1. Spatial distribution of globular clusters at high redshifts

Before discussing the detailed properties of the model clusters, we first consider their spatial distribution. Figure 1 shows the density and temperature maps, as well as the velocity field of gas, in the region of the most massive disk at  $z = 4$ . Globular clusters identified within their parent molecular clouds are represented by circles in the density map. The figure shows that clusters in our model form in the very dense cold regions, generally tracing the spiral arms of the galaxy. The morphology of the distribution is very similar to that of young stellar clusters observed in starburst galaxies (e.g., Whitmore & Schweizer 1995; Zhang et al. 2001). At this epoch the parent halo of the disk experiences frequent mergers and vigorous accretion of fresh gas. The two cold knots outside the spiral arms, for instance, are the small-mass satellite galaxies in the process of merging with the central halo. The gas in these satellites is very dense and could have been compressed by the external pressure and shocks accompanying their collision with the disk. The galaxy as a whole exhibits frequent bursts of star formation associated with the minor and major mergers.

Figure 2 shows the spatial distribution of model globular clusters within the large-scale structure formed in our simulation at  $z = 7$  and  $z = 4$ . The distribution of dark matter is typical of hierarchical models. Visually, it is dominated by prominent filaments on large scales and hundreds of dense dark matter halos tracing these filaments on small scales. The figure shows that parent halos of globular clusters are tracing the skeleton of the large-scale structure. They concentrate in the densest regions of the filaments close to the central massive object. In other words, the distribution of halos forming clusters is highly biased with respect to the overall distribution of matter. This bias is especially pronounced at  $z = 7$ . The highly clustered distribution of halos at the early epochs is a generic feature of the hierarchical models, in which objects of galactic mass correspond to the relatively high peaks in the initial Gaussian density field. This property can be extremely important for explaining the present distribution of globular clusters in the halo of the Milky Way. The high spatial bias of globular clusters at early epochs would result in the more concentrated radial distribution of globular clusters compared to the dark matter today (West 1993) and in the preferential location of higher-metallicity clusters towards the center, in agreement with observations (Djorgovski & Meylan 1994; van den Bergh 2003).

Note that although the high-redshift globular clusters form in dense gaseous disks, the subsequent accretion of their parent galaxies along filaments will lead to tidal stripping and disruption. The clusters are likely to share the fate of the stripped stars of the disrupted galaxies that build up galactic stellar halo and should therefore have similar spatial distribution at  $z = 0$ . We will investigate dynamical evolution and the present-day spatial distribution of the GC population in our model in a future study.

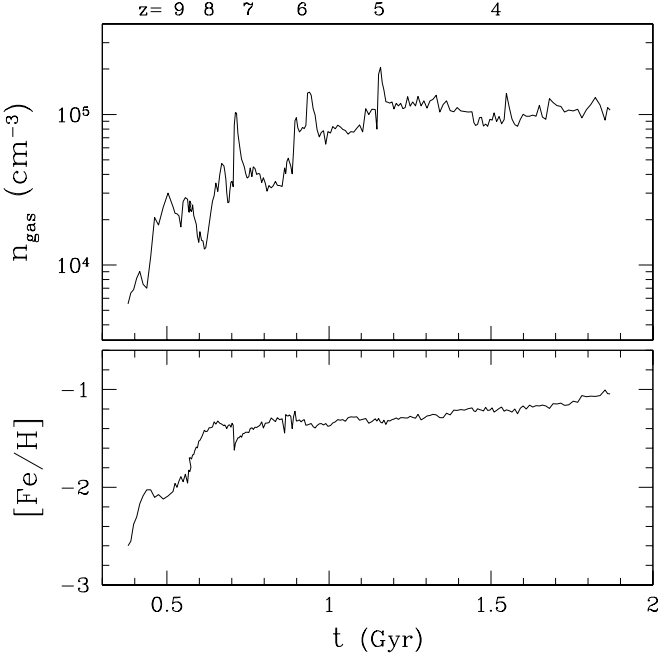


Fig. 3.1. Accretion history in the central cell of the main progenitor halo. Upper panel: Gas number density. The density of dark matter and stars in this region is an order of magnitude smaller. Lower panel: Iron abundance of the gas with respect to the solar value. The metallicity is due to SN II enrichment, as the contribution of SN Ia is negligible at these epochs.

### 3.2. Molecular clouds in the dense high-redshift disks

The globular clusters in our model form in the high-density cores of giant molecular clouds of the high-redshift galaxies (Fig. 1). It is therefore important to consider the properties of the molecular clouds in connection to the properties of globular clusters and host galaxies. Figure 3 shows the evolution of density and metallicity in the central cell of the most massive disk shown in Figure 1. Although this cell has the highest gas density and is located at the bottom of potential well, some of the evolutionary features are illustrative. The gas density exhibits several prominent peaks associated with the fast episodes of accretion. The cold metal-poor gas is delivered to the center of the disk both by merging of smaller galaxies and by direct accretion of gas along a filament that reaches inside the disk region. The rapid increase of the density and pressure in the cell during the accretion events can trigger the collapse of the molecular cloud. The evolution becomes milder at lower redshifts ( $z > 5$ ) as the accretion of gas to the center of the disk slows down.

The bottom panel of Figure 3 shows the evolution of metallicity due to the SN ejecta (the contribution of SN Ia to the metallicity is negligible at these epochs). The metallicity quickly increases to about 10% of solar and then evolves slowly. Note that the events of accretion of the fresh low-metallicity gas may lower the mean metallicity, even in the very central region. If a series of globular clusters forms between  $z = 8$  and 4 in this region, the younger ones are not necessarily more metal-rich than the older ones. Overall, the galaxies in the simulation exhibit a well-defined correlation between the stellar mass and the average metallicity of stars,  $Z / M^{0.5}$ , similar to the correlation observed in nearby dwarf galaxies (Dekel & Woo 2003). There is also a significant spread in gas metallicity even within a single object, which indicates that mixing of metals is rather efficient. The wide range of gas metallicity in star forming regions eliminates any clear age-metallicity correlation for high-redshift clusters. For instance, stars formed at the same epoch can have metalicities different by up to two orders of magnitude. This may also at least partially explain the well-known "second parameter problem" (e.g., Carney 2001).

The efficiency of GC formation, i.e. the ratio of the globular cluster mass to the mass of the molecular, baryonic, or dark matter system containing it, depends on the averaging scale. Within the cores of giant molecular clouds the local efficiency is of the order unity ( $\approx 2.4$ ). Averaged over the whole molecular cloud though, the efficiency is much lower because most of the molecular gas is not participating in star formation at any given time. When compared with the total gas and/or dark matter mass in the galaxy, the efficiency decreases by another order of magnitude. There are thus various types of globular cluster formation efficiencies, which we consider in turn.

The detailed properties of the simulated molecular clouds depend on the threshold density,  $\rho_{th}$ , used to define the cloud boundary (see § 2.3). This boundary can be thought of as an external tidal limitation. The mass and size of the cloud increase with the decreasing threshold density. The cloud-scale efficiency of globular cluster formation, which we define as  $\eta_{GC} = M_{GC} / M_{cloud}$ , varies accordingly. We find that the average efficiency is about  $10^{-2}$  for  $\rho_{th} = 50 M_{\odot} pc^{-3}$ , is in the range  $10^{-3} - 10^{-2}$  for  $\rho_{th} = 10 M_{\odot} pc^{-3}$ , and  $10^{-4} - 10^{-3}$  for  $\rho_{th} = 1 M_{\odot} pc^{-3}$ . The estimated masses of globular clusters, on the other hand, depend only on the properties of the cloud cores and are insensitive to the changes in the external boundary condition.

For the massive globular clusters with  $M > 3 \times 10^5 M_{\odot}$  and the associated massive molecular clouds in our fiducial model with  $\rho_{th} = 1 M_{\odot} pc^{-3}$ , the formation efficiency is roughly constant:  $\eta_{GC} = 10^{-3}$ . However, if we include lower mass clusters we find an anti-correlation with the cloud mass (Spearman correlation coefficient  $r_s = -0.35$ ). In the range  $10^5 M_{\odot} < M_{cloud} < 10^8 M_{\odot}$ , the relation is  $\lg \eta_{GC} = 1.6 (0.22 \pm 0.02) \lg (M_{cloud}/M_{\odot})$ . Overall, the numerical values of the efficiencies we obtain are in good agreement with observations (Harris & Pudritz 1994).

Ashman & Zepf (2001) suggested that the formation efficiency scales with the binding energy of the molecular cloud,  $\eta = (M_{cloud}/R_{cloud})^{1/2}$ ,  $\eta = 0.75 - 0.25$ . Alternatively, using the observed relation for the masses and sizes of molecular clouds in the Galaxy,  $M_{cloud} / R_{cloud}^2$  (Larson 1981), this scaling can be rewritten as  $\eta = (M_{cloud}/R_{cloud}^3)^{1/2}$ . Note that the proposed relation implies an anti-correlation with the density of the cloud:  $\eta \propto (M_{cloud}/R_{cloud}^3)^{1/2}$ , i.e. the less dense clouds form stars more efficiently. We do not find such trend: for small clusters we find the anti-correlation of  $\eta$  with  $M_{cloud}$  ( $\eta \propto M_{cloud}^{-1/2}$ ), and for large clusters  $\eta \approx \text{const.}$

### 3.3. The global efficiency of globular cluster formation

An important measure of the efficiency of globular cluster formation is the total mass of clusters,  $M_{GC}$ , within a parent galactic halo. For example, in giant elliptical

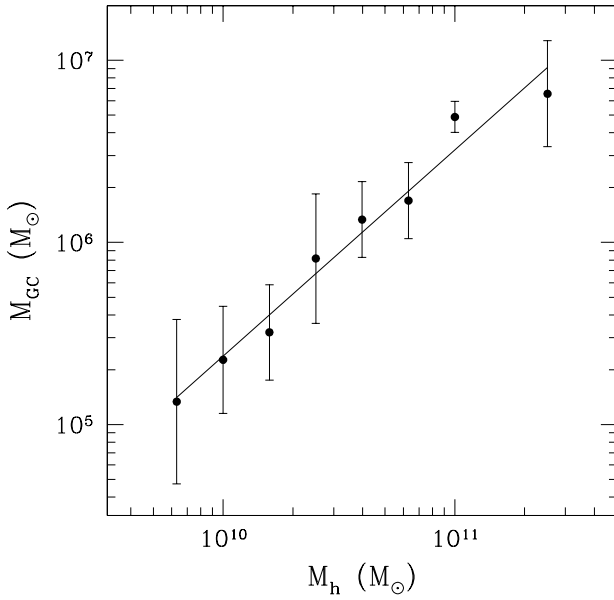


Fig. 4.| The mass of the globular cluster system within a given halo vs. the total mass of its parent halo, combined over all analyzed epochs. Dots show the average in bins of width  $\lg M_h = 0.2$ , while the error bars show the 1 $\sigma$  deviations within the bin (not the error of the mean). The solid line is the least-squares fit with the slope  $d \lg M_{GC} = d \lg M_h = 1.13 \pm 0.08$ .

galaxies the ratio of the total cluster mass to the mass of stars plus the hot X-ray emitting gas is roughly constant,  $\frac{M_{GC}}{M_h} = 0.0026 \pm 0.0005$  (McLaughlin 1999). This parameter can be thought of as the efficiency of the conversion of baryons into globular clusters. In massive objects the baryon mass  $M_b$  relates to the total galaxy mass  $M_h$  via the universal baryon fraction,  $M_b = M_h \cdot f_b = 0.14$ . Thus perhaps even more fundamental is the ratio of the globular cluster mass to the total galaxy mass:  $\frac{M_{GC}}{M_h} = 0.0026$ .

Figure 4 shows the sum of the globular cluster masses in each halo versus the progenitor galaxy mass. There is a well-defined correlation of the form

$$M_{GC} = 3.2 \cdot 10^6 M_h^{1.13 \pm 0.08} \quad (6)$$

albeit with scatter. The global efficiency  $\frac{M_{GC}}{M_h}$  is therefore only weakly dependent on the galaxy mass. For most halos harboring massive clusters we find  $\frac{M_{GC}}{M_h} = (2 \pm 5) \cdot 10^{-5}$ . The global baryon efficiency is in the range  $\frac{M_{GC}}{M_h} = (2 \pm 3) \cdot 10^{-4}$ , and it scales with the galaxy mass as

$$\frac{M_{GC}}{M_h} = 2.5 \cdot 10^{-4} \cdot M_h^{0.25 \pm 0.12} \quad : \quad (7)$$

While these values are lower than those found by McLaughlin (1999), they are in fact appropriate for a spiral galaxy like our own. McLaughlin (1999) derived  $\frac{M_{GC}}{M_h} = 0.0027$  for the Galaxy taking into account only the mass of the stellar spheroid. We are interested here in scaling with the total mass and therefore take the most recent estimate of the virial mass of the Milky Way  $M_h = 10^{12} M_\odot$  (Klypin et al. 2002). The mass of the observed globular clusters is  $M_{GC} = 5.2 \cdot 10^7 M_\odot$  (Harris 1996), and as McLaughlin (1999) argues, this mass cannot differ from the initial

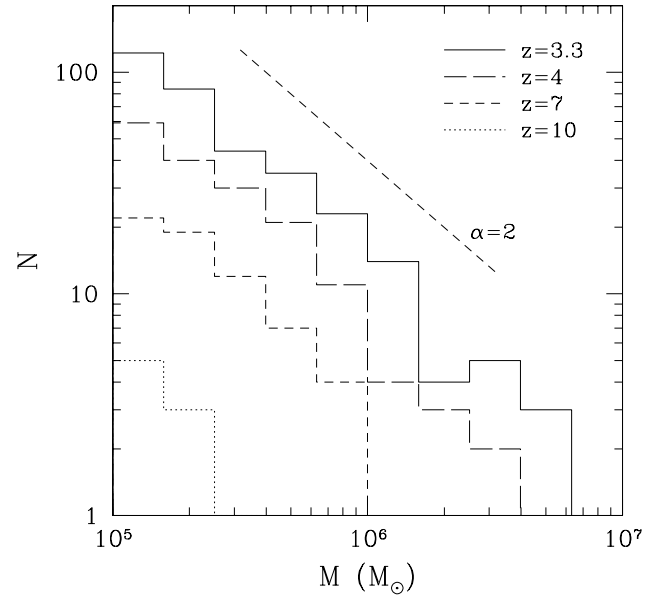


Fig. 5.| The build-up of the initial mass function of globular clusters. Dotted, dashed, long-dashed, and solid histograms show cumulative distributions at  $z = 10, 7, 4$ , and  $3.3$ , respectively. The straight dashed line shows a power-law,  $N \propto M^{-\alpha}$ , with a slope  $\alpha = 2$ . Note that this is the mass function of the young clusters and dynamical evolution effects are not accounted for. These effects will be discussed in x 6 (see Fig. 13).

mass by more than 25%. Thus the global efficiency for the Galaxy is  $\frac{M_{GC}}{M_h} = 5 \cdot 10^{-5}$ , and the baryon efficiency  $\frac{M_{GC}}{M_h} = f_b = 4 \cdot 10^{-4}$ . Both of these estimates agree with our derived correlations, eqs. (6) and (7).

It is interesting also that the mass of the globular cluster population and the maximum cluster mass in a given region strongly correlate with the local average star formation rate density:  $M_{max} / \frac{SFR}{SFR} = 0.54 \pm 0.07$  and  $M_{GC} / \frac{SFR}{SFR} = 0.75 \pm 0.06$  at  $z = 3.3$ , where the masses and star formation rate were estimated taking into account clusters ( $M > 5 \cdot 10^4 M_\odot$ ) and stellar particles younger than  $5 \cdot 10^7$  yrs and averaging over the cells of 7.7 physical kpc. Each averaging cell therefore represents a different progenitor galaxy in the simulation. A similar correlation, albeit with a significant scatter, was reported for the observed present-day galaxies (Larsen 2002). The interpretation of this correlation is straightforward in our model. The star formation rate depends sensitively on the mass fraction of gas in cold high-density star forming regions (Kavtsov 2003b). The massive clusters in our model are also assumed to form in such regions. Thus, both the star formation rate and mass of the globular cluster population are controlled by the amount of gas in the densest regions of the ISM.

### 3.4. The mass, size, and metallicity distributions of the model clusters

Figure 5 shows the mass function of the model clusters identified in all output epochs prior to a given redshift. The distribution is well fit by a power-law  $dN/dM \propto M^{-\alpha}$  at  $M > 10^5 M_\odot$ . The slope becomes shallower with decreasing redshift and saturates at  $\alpha = 2.05 \pm 0.07$  for

Table 1  
The quartiles of the size and metallicity distributions of the model and Galactic globular clusters

|                  | $R_h$ (25%) | $R_h$ (50%) | $R_h$ (75%) | [Fe/H] (25%) | [Fe/H] (50%) | [Fe/H] (75%) |
|------------------|-------------|-------------|-------------|--------------|--------------|--------------|
| $z = 10$         | 1.9         | 2.0         | 2.3         | -2.7         | -2.6         | -2.5         |
| $z = 7$          | 2.0         | 2.4         | 2.7         | -2.2         | -1.8         | -1.6         |
| $z = 4$          | 2.0         | 2.4         | 2.9         | -1.8         | -1.5         | -1.2         |
| $z = 3.3$        | 2.0         | 2.3         | 2.9         | -1.7         | -1.4         | -1.1         |
| M W, [Fe/H] < -1 | 1.2         | 2.8         | 4.8         | -1.8         | -1.6         | -1.4         |
| M W, all         | 0.7         | 2.4         | 4.0         | -1.7         | -1.4         | -0.7         |

$z = 4$ . We do not account for the effects of dynamical evolution on the mass function here, but discuss them in §6. In this and subsequent figures we discard the most massive cluster identified at the center of the most massive disk. Such cluster would be identified in observations as a bright galactic nucleus rather than a distinct globular cluster.

The simplicity of the global power-law shape of the mass function is deceiving, as the mass functions of clusters in individual galaxies exhibit a variety of shapes. Figure 6 shows, for example, that small halos form only clusters with  $M < 10^6 M_\odot$  with the mass function slope steeper than  $\alpha = 2$ , while large halos form more massive clusters with a shallower mass function. Remarkably, the convolution of the halo distribution with the distribution of clusters within each halo produces the seemingly invariant power-law mass function of globular clusters. We investigate the detailed shape of the mass function and its origin in §4.

Figure 7 shows the distribution of the half-mass radii, calculated according to our subgrid model as  $R = R_{sf} =$ . In this and the following figure we plot only the massive clusters,  $M > 10^5 M_\odot$ , expected to survive the dynamical evolution. The model distribution is generally similar to the observed sizes of the Galactic globular clusters (c.f., van den Bergh 1996). The differences at the smallest and largest ends can be due to the following effects. The adiabatic expansion condition may not apply to the most massive clusters which would then be larger. The dynamical evolution effects, on the other hand, would shrink the clusters and fill the range  $R < 1$  pc. Also, some of the surviving clusters with  $M < 10^5 M_\odot$  may contribute to the smallest size bin as well.

Figure 8 shows the distribution of cluster metallicities, which is remarkably similar to the metal-poor part of the Galactic cluster distribution (see Table 1). Interestingly, we do not find any correlation between the mass and metallicity of globular clusters. The Spearman rank correlation coefficient for the cumulative distribution at  $z = 3.3$  is  $r_s = 0.06$ , which is consistent with no correlation. Similarly, there is no correlation for the Galactic GCs (Djorgovski & Meylan 1994). The absence of the mass-metallicity correlation may be due to a wide range of gas metallicities in the star-forming regions. As we mentioned above,

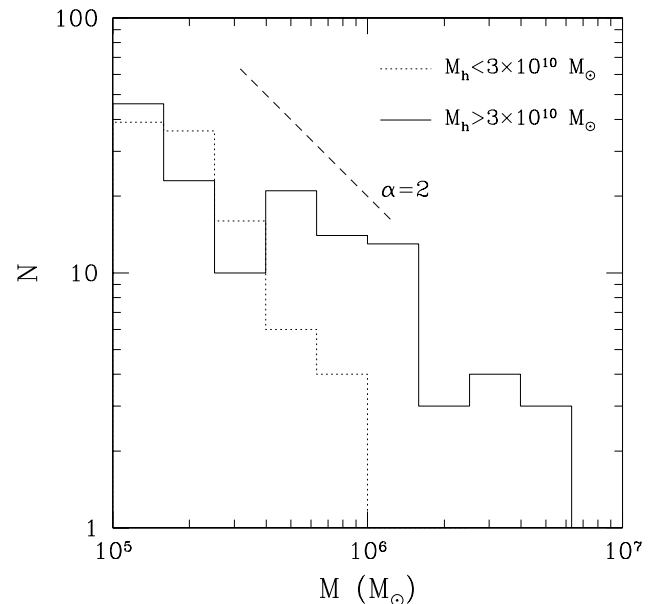


Fig. 6. The mass function of globular clusters formed within the parent halos of mass  $< 3 \times 10^{10} M_\odot$  (dotted histogram) and  $> 3 \times 10^{10} M_\odot$  (solid histogram) at  $z = 3.3$ .

this also explains the lack of a well-defined age-metallicity correlation.

At the high redshifts considered here, most of the metals are contributed by SN II which underproduce iron compared to the  $\alpha$ -peak elements. In order to calculate the fraction of ejected metals contributed by iron,  $[Fe]$ , we use the iron yields of Woosley & Weaver (1995), integrated over the Müller & Scalo (1979) IMF in the range 12 to 40  $M_\odot$ . For the intermediate 'case B' yield models and the assumed solar ratio of iron to hydrogen of  $1.8 \times 10^{-3}$  by mass (Anders & Grevesse 1989), we obtain  $[Fe] = 0.6$ . This estimate is consistent with the enhanced ratios  $[Fe] = 0.3$  observed for the globular clusters in the Galaxy (Carney 1996; Lee & Carney 2002; Smith et al. 2002), M 87 (Cohen et al. 1998), and M 49 (Cohen et al. 2003). The conversion from the total metallicity due to SN II to the iron abundance is  $[Fe/H] = \log([Fe]_{II}/Z) = \log([Fe]/Z) - 0.6$ .

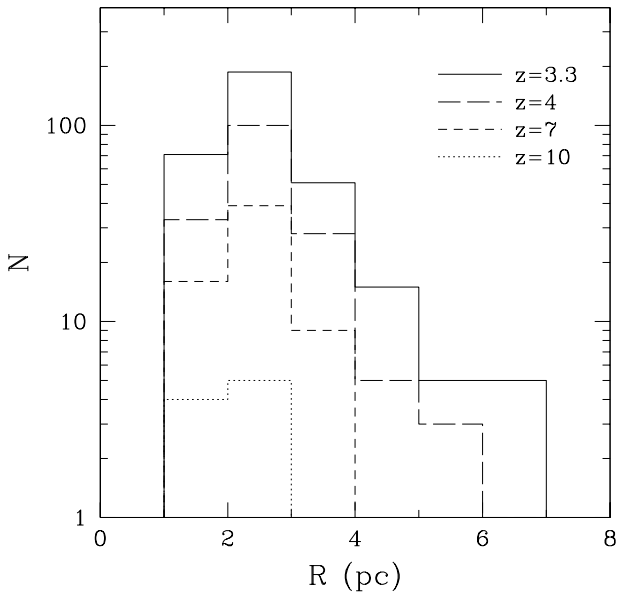


Fig. 7.1 The size distributions of globular clusters at four successive epochs, using only the massive clusters,  $M > 10^5 M_{\odot}$ .

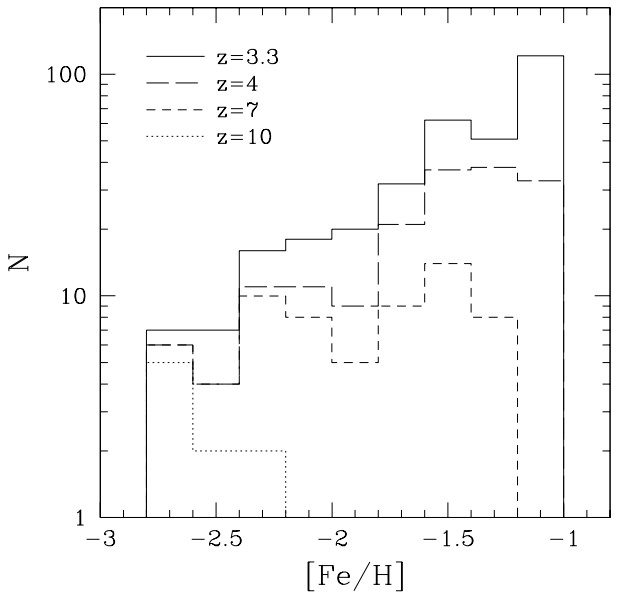


Fig. 8.1 The metallicity distributions of globular clusters at four successive epochs, using only the massive clusters,  $M > 10^5 M_{\odot}$ .

Table 1 compares the medians and the 25% and 75% quartiles of the size and metallicity distributions of the model clusters against the corresponding distributions for the Galactic GC (Harris 1996). There is good agreement between our predictions and the observations. It is plausible that small discrepancies for the smallest sizes and highest metallicities can be explained by subsequent evolution of the cluster population at  $z < 3$ , which we discuss in x 7.1. Note that the evolution can also modify the quartiles of the distribution. We therefore show in Table 1 both

the quartiles for all Galactic clusters and for the clusters with metallicities in the same range as in our model (i.e.,  $[\text{Fe/H}] < -1$ ). It is also interesting that in agreement with observations no clusters are formed with very low (Pop III) metallicities.

Note that at all epochs the dynamical time of the parent molecular cores is very short ( $\sim 10^6$  yrs), which means that the galactic gas is pre-enriched even before the first clusters form. It follows then that the oldest globular clusters do not contain the oldest stars in the Galaxy. As we noted in x 3.2, the galaxies in the simulation exhibit a well-defined correlation between the stellar mass and the average metallicity of stars,  $Z / M^{0.5}$ . Average metallicities of globular clusters are similar to those of the overall stellar population at high redshifts. The model clusters thus follow a similar correlation with the stellar mass and luminosity of their parent galaxy, although with larger spread.

The lack of the metal-rich clusters in our model compared to the Galactic clusters (c.f. Table 1) is likely to be explained by the clusters forming in the higher-metallicity gas at  $z < 3$  (see x 7.1), not accounted for in our analysis. It should be noted, however, that a significant spread in metallicity distributions exists for different galaxies (e.g., Harris 2001) and certain differences with the simulated system are expected. This issue can be addressed in future studies by simulating globular cluster systems in a number of galaxies.

#### 4. the origin and universality of the globular cluster mass function

One of the best studied and perhaps the most important characteristics of globular cluster systems is their mass function (GCMF). The mass function of young star clusters in normal spiral galaxies (e.g., Elmson & Fall 1985; Larsen 2002) and interacting galaxies (e.g., Whitmore et al. 1999; Zhang & Fall 1999; Zepf et al. 1999) can be approximated by a power-law  $dN/dM \propto M^{-\gamma}$  with  $\gamma = 1.5 - 2$  over a large range of masses. Interestingly, the mass function of molecular clouds in the Galaxy can also be described by the power-law with a similar slope (Solomon et al. 1987). In addition, the power-law slope of the high-mass tail of the GCMF resembles that of the high-redshift mass function of dark matter halos in the hierarchical CDM cosmology (Press & Schechter 1974; Sheth & Tormen 1999). In this section we consider the origin and universality of the cluster mass function in relation to the mass function of giant molecular clouds and parent halos.

Gnedin (2003) used a simple semi-analytic model in which a single massive cluster dominates the mass of the globular cluster system within a progenitor halo:  $M_{\text{max}} \propto M_{\text{GC}}^{1/2} f_b M_h$  (c.f. x 3.3). The model implies that the shape of the high-mass tail of the GCMF simply reflects the shape of the mass function of progenitor halos of the Milky Way at high redshifts. This direct connection between the cluster and halo mass functions is due to the assumption that GC properties are determined solely by the mass of their parent halo. This key assumption can be tested against the results of our simulation.

We find indeed that the most massive cluster contributes a significant fraction of the total cluster mass. The average for all halos is  $M_{\text{max}} \approx 0.6 M_{\text{GC}}$ . In x 3.3 we have shown that  $M_{\text{GC}}$  is roughly proportional to the parent galaxy

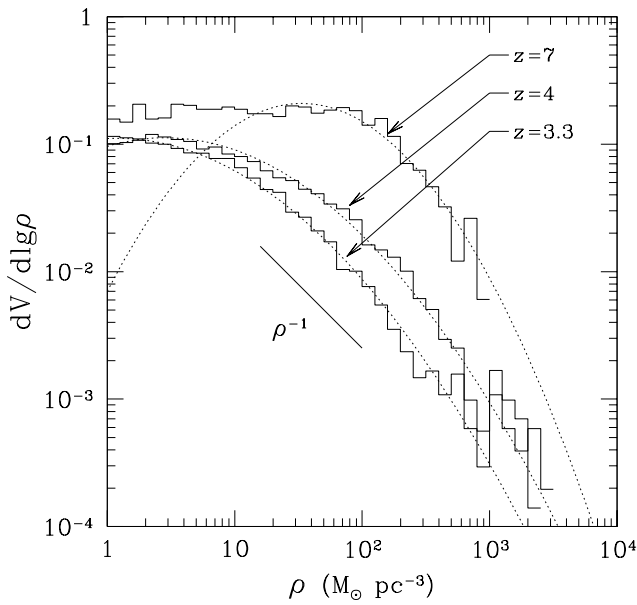


Fig. 9. Probability distribution function of the gas density (fraction of the total volume occupied by the cells in a given density range) for the highest level of refinement at  $z = 4$ . The dotted lines show the log-normal fits to the highest-density tails of the distribution, in the range  $1 - 10^3 M_{\odot} pc^{-3}$  for four epochs. The straight line shows the slope  $dV/dlg \rho \propto \rho^{-1}$ .

mass, and therefore a similar relation exists for the most massive clusters:

$$M_{\max} = 2.9 \cdot 10^6 M_{\odot} \quad \frac{M_h}{10^{11} M_{\odot}} \quad : \quad (8)$$

However, a significant scatter around this average relation implies that for a given halo the masses of individual clusters can vary by a factor of three. Also, the normalization corresponds to the global efficiency of cluster formation  $M_{\max} \approx 4 \cdot 10^4$  (see 3.3, an order of magnitude below the value found by McLaughlin (1999)). This result implies that the mass function of globular clusters does not follow directly from the mass function of their parent halos.

Instead, we find that the overall shape of GCMF in our model is determined by both the mass function of progenitor halos and the mass function of molecular cloud cores within individual galaxies. The latter, in turn, is determined by the structure of the galaxy disks. Kavtsov (2003b) showed that the density probability distribution function (PDF) of the galactic disks in our simulation, defined as the fraction of the volume in a given logarithmic density interval, can be described by a log-normal function at the high gas densities typical for molecular clouds. Figure 9 shows the density PDF measured in the simulation at  $z = 7, 4$ , and  $3.3$ , using only the highest refinement level ( $l=9$ ) cells which cover the galactic disks and include the sites of GC formation. The log-normal distribution provides a very good fit to the high density tail of PDF at  $\rho > 1 M_{\odot} pc^{-3}$ :

$$\frac{dN}{d \lg \rho} \propto \exp \left( \frac{(\lg \rho - \lg \rho_0)^2}{2^2} \right) : \quad (9)$$

The characteristic density  $\rho_0$  and the dispersion of the log-normal PDF vary with redshift. The characteristic

density decreases from  $\lg \rho_0 = 1.8$  at  $z = 8$  to  $0.08$  at  $z = 3.3$ , while the width of the distribution increases from  $0.46$  to  $0.85$  over the same redshifts. The evolution in this redshift interval can be fitted by  $\lg \rho_0 = 3.30 (1.41 \cdot 0.02) [10 = (1+z)]$  and  $\sigma = 1.23 (0.83 \cdot 0.05) [10 = (1+z)]$ .

Figure 9 shows also that over a limited density range,  $1 < \lg \rho < 3$ , the PDF can be described by a power-law

$$\frac{dN}{d \lg \rho} \propto \rho^{-n} \quad (10)$$

with  $n = 1.08 \cdot 0.06$  (for  $z = 4$ ). Over a wider range of densities, however, the log-normal function is a better description of the PDF. For instance, the power-law slope becomes steeper with increasing density: we find  $n = 1.26 \cdot 0.08$  for  $\lg \rho > 1.5$  and  $n = 1.41 \cdot 0.13$  for  $\lg \rho > 2$ . The latter range includes the molecular cloud cores in which the most massive clusters ( $M > 10^5 M_{\odot}$ ) form in our model.

The characteristic shape of the PDF from Figure 9 has been found in several numerical studies of the turbulent ISM. In particular, it is very similar to the density PDF in the 2D disk simulations of Wada & Norman (2001). Scalo et al. (1998) showed that the power-law PDF tail arises in non-isothermal supersonic turbulent flows, while the log-normal distribution is thought to be a generic feature of isothermal flows (e.g., Vazquez-Semadeni 1994; Padoan et al. 1997; Vazquez-Semadeni et al. 2000). For the heating/cooling rates adopted in our simulation the gas at densities  $\rho \gtrsim 5 M_{\odot} pc^{-3}$  is nearly isothermal, which may explain why the log-normal distribution provides a better fit to the high-density tail of the PDF than the power-law. The log-normal shape of the distribution is likely to be due to the chaotic nature of the supersonic turbulent flows, characterized by numerous random convergent flows and shocks. The evolution of individual gas elements can be thought of as a random walk in density leading to the log-normal equilibrium distribution (Bialek 2002). The width of the PDF for the isothermal gas is proportional to the rms Mach number (Padoan et al. 1997). The widening of the PDF with time can therefore be a result of the hierarchical assembly of galaxies and the increase of the rms velocity dispersion of gas clouds.

Globular clusters in our model form only in the highest-density cores of the identified molecular clouds which represent a subset of all high-density cells. Nevertheless, we find that the PDF of the cores (or density peaks) is similar to the overall PDF at  $\lg \rho > 0$ . The Kolmogorov-Smirnov test of the unbinned probability distributions shows that the differences between the core and the overall PDFs are not statistically significant. At all epochs the probability that the two PDFs are drawn from the same distribution is at least 13%. This indicates that the density PDF of the cores is also described by the same log-normal distribution. The density of each core determines the mass of the globular cluster it hosts. The density PDF of the cores thus determines the mass function of globular clusters.

Given our subgrid model, the cluster mass scales with the core gas density as  $M \propto \rho^{3/2}$  (eq. [5]). For a power-law density PDF the expected cluster distribution is  $dN \propto dM \propto M^{-1/2n-3}$ , or  $\rho = 1 + 2n = 3$ . For  $n = 1$  this gives the slope  $\rho = 5 = 1.7$ , while for  $n = 1.4 \cdot 0.13$ , appropriate for the highest-density tails of the PDF and the most massive clusters,  $\rho = 1.94 \cdot 0.09$ , in good agreement with

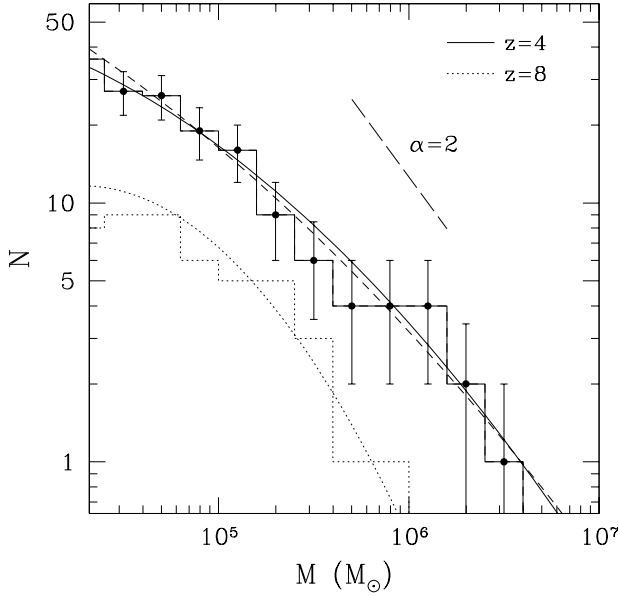


Fig. 10. Mass function of globular clusters forming at two epochs (histograms) with the superimposed fit (smooth solid and dashed lines) from the density PDF distribution (eq. [11]). The error bars represent the Poisson errors /  $N^{1/2}$ . The dashed line shows the mass function calculated from the density PDF of the lower,  $l=8$ , level of refinement normalized to the same total number of clusters.

the mass function slope seen in Figure 5. Therefore, we can expect a relatively shallow,  $\sim 1.7$ , mass function for the small-mass clusters forming in lower-density cores and the steep,  $\sim 2$ , mass function for massive globular clusters forming in the densest regions of the disk. The range of slopes derived in our model is in close agreement with observations (Whitmore & Schweizer 1995; Meurer et al. 1995; Elmegreen & Elmegreen 1997). The steepening of the luminosity function with increasing luminosity is also observed for young star clusters in starbursting and interacting galaxies (Whitmore et al. 1999; Larsen 2002).

From our analysis above it is clear that the power-law is not the best description of the mass function. The log-normal shape of the density PDF implies the log-normal mass function:

$$\frac{dN}{d \lg M} = N_0 \exp \left( \frac{(\lg M - M_0)^2}{2 M^2} \right) \quad (11)$$

with  $M = \frac{3}{2}$  and  $M_0 = M(\rho_0)$  using equation (5). We find that at all epochs this functional fit provides a better description of the cluster mass function than a single or a double power-law. Figure 10 shows the mass function of clusters at  $z=8$  and  $z=4$  along with the log-normal function calculated from the best fit to the density PDF. In other words, the smooth lines in the figure represent not fits to the mass function, but the fits to the PDF converted to the mass function using our subgrid model.

Although many progenitor halos contribute their globular clusters to the total mass function, the log-normal distribution also describes the mass function of clusters of a single galaxy. Figure 11 shows the mass function of clusters identified at  $z=4$  within the virial radius of the

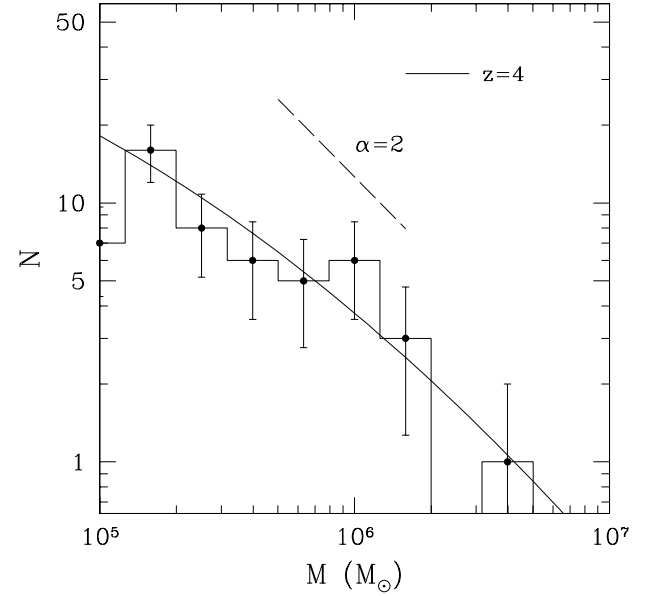


Fig. 11. Mass function of globular clusters forming between redshifts  $z=4$  and  $3.6$  within the virial radius of the most massive galaxy, with the superimposed fit from the density PDF distribution (eq. [11]).

most massive progenitor, along with the log-normal distribution given by equation (11) with  $M_0 = 1.3 \cdot 10^3 M_\odot$  and  $M = 1.2$ . The log-normal distribution describes the mass function well within the Poisson errors, while it is clear from even a quick examination of the plot that the mass function cannot be well fit by a single slope power-law.

The parameters of the distribution,  $M_0$  and  $M$ , follow directly from the parameters of the density PDF. As redshift decreases, the characteristic peak  $\rho_0$  decreases and the dispersion increases. While their exact values at a given redshift may be specific to our simulated galaxy, i.e. depend on the environment, the anti-correlation between the parameters may be more general. We find the following relation which can be tested by future simulations and observations:

$$\lg M_0 = (6.2 \pm 0.5) - (2.8 \pm 0.5) \lg M \quad (12)$$

These results apply to the mass function of young stellar clusters not modified by dynamical evolution. The mass function of young star clusters in observations is often fit by a double power-law distribution (e.g., Whitmore 2000). Such a function has four free parameters, whereas the log-normal distribution has only three free parameters, including the normalization. Therefore, it is not only more accurate but also simpler than the double power-law. We argue also that the log-normal mass distribution reflects the underlying density distribution of molecular cloud cores and is therefore physically motivated.

In order to illustrate that the log-normal distribution can fit the observations, we plot on Figure 12 the mass function of young ( $25 < t < 160$  Myr) stellar clusters in NGC 4038/9 (the "Antennae"), as derived by Zhang & Fall (1999). This figure demonstrates that the log-normal function describes the observed mass function better than the power law. The best fit power-law slope is  $\sim 2.01$

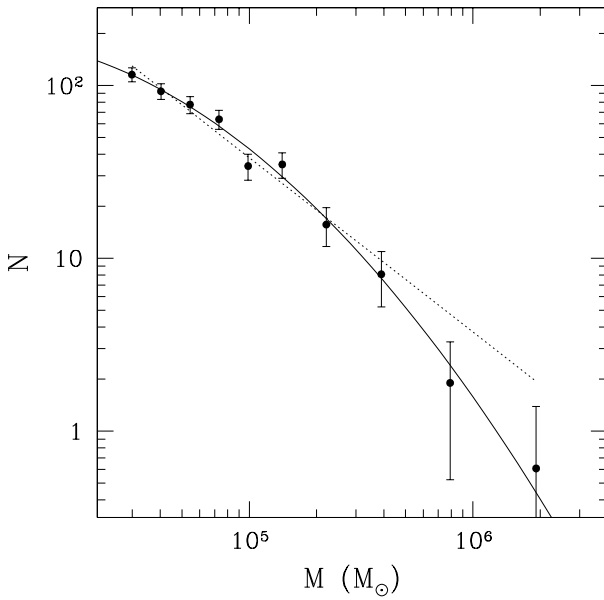


Fig. 12.1 The mass function of young (age  $25 < t < 160$  M yr) stellar clusters (solid circles with error bars) in NGC 4038/9 (the 'Antennae'), as derived by Zhang & Fall (1999) and the best fits of the power law (dotted line) and log-normal (solid curve) mass distributions.

0.07 with the reduced  $\chi^2 = 1.17$ , while the error of the log-normal fit is almost twice as good,  $\chi^2 = 0.68$ . The parameters of the fit,  $\lg M_0 = 3.7 \pm 0.4$  and  $\alpha_M = 0.73 \pm 0.12$ , are in reasonable agreement with the derived relation (12), especially if we take into account the difference in redshifts, metallicity, and environment.

The results presented in this section indicate that the observed luminosity and mass functions of young clusters could be described by a power-law simply due to the limited range of luminosities typically probed in observations (2–4 magnitudes or only about a factor of 10–40 in mass; Elmegreen & Elmegreen 1997; Whitmore 2000). The second implication is that the power-law slope should steepen at the highest cluster masses:  $M \gtrsim 10^7$  M<sub>sun</sub>. This, in turn, implies that there exists a maximum cluster mass at any given epoch. This is an important conclusion as it may explain the characteristic masses of clusters in the Local Group.

##### 5. numerical convergence

The numerical resolution of the simulation in any numerical study invariably places constraints on the validity of the results. The spatial and mass resolution of the gas element in our adaptive mesh simulation is set by the maximum level of refinement. In our simulation  $l_{\max} = 9$  was determined by the available computational resources. We can check, however, how the results would change if we limited the maximum level to  $l = 8$ . This corresponds to a factor of 8 lower mass resolution and a factor of two larger cells.

We find that the density PDF of the  $l = 8$  cells can be well fit by a log-normal function but with a correspondingly lower characteristic density  $\rho_0$ . The dispersion is consistent with that for  $l = 9$  level within the errors.

The mass function resulting from the  $l = 8$  density PDF is therefore somewhat steeper than for the  $l = 9$  cells, because  $M_0$  is lower and the same mass interval of globular clusters falls on the steeper part of the log-normal function. The difference, however, is only apparent at very low masses ( $M \lesssim 3 \times 10^4$  M<sub>sun</sub>).

The dashed line in Figure 10 shows the cluster mass function expected for the density PDF of the  $l = 8$  cells normalized to the same number of clusters as the  $l = 9$  mass function. It fits the histogram of the model clusters equally well. The deviation only becomes significant at  $M < 3 \times 10^4$  M<sub>sun</sub>. Thus, the shape of the derived mass function converged at masses higher than  $3 \times 10^4$  M<sub>sun</sub>.

The number of model clusters is of course uncertain and depends both on the choice of formation sites and the particular distribution of molecular clouds. Although the spatial resolution of our simulation is very high by the standards of cosmological simulations, the molecular clouds are resolved only marginally. This results in a certain ambiguity in defining the clouds and the total number of forming clusters. The abundance of globular clusters in our model can therefore be viewed as a tunable free parameter. However, all results concerning the distributions of cluster properties should be considered as the predictions of the model.

##### 6. dynamical evolution

In contrast to the mass function of young clusters, the mass function of Galactic and most extragalactic globular clusters has traditionally been described by a Gaussian function of magnitudes:

$$\frac{dN}{d\lg M} / \exp \left( \frac{(\lg M - \lg M_{\text{peak}})^2}{2^2} \right); \quad (13)$$

where  $M_{\text{peak}} = 2 \times 10^5$  M<sub>sun</sub> and  $\sigma = 0.5$  (we use the mass function and the luminosity function for old clusters interchangeably, assuming a constant mass-to-light ratio  $M = L_V = 3$  in solar units). Alternatively, the GCMF can be represented by two power-laws  $dN/dM \propto M^{-\alpha}$ , with

2 for  $M > M_{\text{peak}}$  and 0.2 for  $M < M_{\text{peak}}$  (McLaughlin 1994; McLaughlin & Pudritz 1996). In order to understand the origin of the cluster mass function, we need to understand both the initial mass function of young clusters and its difference from the observed mass function of old clusters. In this section we discuss the secular dynamical evolution of globular clusters, apply a simple evolutionary model to the globular clusters in the simulation, and compare the resulting distribution to the mass function of the Galactic globular clusters.

Sophisticated models of the dynamical evolution started by Spitzer and collaborators in the 1970s (see Spitzer 1987) and refined in the 1990s (Chernoff & Weinberg 1990; Gnedin & Ostriker 1997; Murali & Weinberg 1997; Vesperini 1998; Gnedin et al. 1999) have shown that tidally-truncated clusters undergo secular mass loss over the Hubble time. Three main processes shaping the GCMF are the evaporation through two-body relaxation, tidal shocking by the host galaxy, and stronger tidal truncation due to dynamical friction. The effects of these processes have been studied extensively and the results of the detailed numerical simulations parametrized for semi-analytic calculations.

Following Gnedin & Ostriker (1997) we define the cluster destruction timescale due to all dynamical processes

as

$$t_d(M, R) = \frac{1}{t_{ev}} + \frac{c_1}{t_{sh}} + \frac{c_2}{t_{df}} \quad ; \quad (14)$$

where  $M$  is the cluster mass and  $R$  is the half-mass radius. The evaporation time scale for tidally-truncated clusters is roughly a multiple of the half-mass relaxation time:

$$t_{ev} = 30 t_{rh} \\ = \frac{7.7 \cdot 10^{10} \text{ yr}}{\ln_{ev}} \frac{M}{10^6 M} \frac{1=2}{\text{pc}} \frac{R}{0.8 M} \frac{3=2}{\text{m}} \frac{1}{0.8 M} \quad (15)$$

where  $\ln_{ev} 0.4 M = m$ , and  $m$  is the typical mass of stars in clusters.

The tidal shocking time scale depends on the properties of the host galaxy. For a spheroidal halo it is  $t_{sh} (V_p R_p^2 / G M_p)^2 P_{orb}^{-1}$ . Here  $V_p$  and  $R_p$  are the velocity and distance of the closest approach to the center, where the enclosed halo mass is  $M_p = M_h < R_p$ . The orbital period of the cluster is  $P_{orb}$ , and the internal angular speed is  $\Omega^2 = 0.4 G M / R^3$ . In order to adapt this equation to our simulated halos with circular velocity  $V_c$ , we estimate  $P_{orb} \approx 2 d/V_c$  and  $V_p R_p^2 / G M_p \approx d/V_c$ , where  $d$  is the distance from the cluster to the center of its parent halo. Note that the latter relation is very approximate. With this caveat in mind, we write the tidal shocking time scale as

$$t_{sh} = 1.1 \cdot 10^{13} \text{ yr} \frac{d}{\text{kpc}}^3 \frac{V_c}{\text{km s}^{-1}}^3 \frac{M}{M} \frac{R}{\text{pc}}^3 \quad ; \quad (16)$$

Finally, the dynamical friction time scale for moderately eccentric orbits can be written as

$$t_{df} = \frac{2.6 \cdot 10^{14} \text{ yr}}{\ln_{df}} \frac{d}{\text{kpc}}^2 \frac{V_c}{\text{km s}^{-1}} \frac{M}{M} \quad ; \quad (17)$$

where  $\ln_{df} = V_c^2 d / G M$  (e.g., Colpi et al. 1999).

The origin of the low-mass end of the GCMF has been discussed by Fall & Zhang (2001). Small-mass tidally-truncated clusters are affected primarily by two-body scattering of stars and the associated expansion. Their mass loss due to such relaxation effects is almost independent of the cluster mass,  $M \approx 10^5 M_{\odot} \text{ yr}^{-1}$  (Vesperini & Heggie 1997; Gnedin et al. 1999), so that the cluster mass decreases linearly with time. This leads to a quasi steady-state solution where  $dN/dM = \text{const}$  (Fall & Zhang 2001), in agreement with observations.

We can therefore describe the evolution of the initial GCMF using a simple model as follows. For the clusters with initial mass  $M$  formed at redshift  $z$  and cosmic time  $t_z$  we define the mass loss as  $M = M(t_0, t_z) = t_d$ . The clusters with  $t_0 < t_z > t_d$  would be completely destroyed and are discarded. The coefficients  $c_1$  and  $c_2$  in eq. (14) account for uncertainty in the properties of the host halos. The galaxy merger rate peaks between redshifts 7 and 4, and each such event may eject the newly formed cluster from the halo. This would affect  $t_{sh}$  and to an even greater extent  $t_{df}$ , because the rate of dynamical friction is high in small-mass halos and is almost negligible in large ones. Reducing the coefficients from their default value of 1 thus reduces the time for the tidal evolution. As a conservative estimate we set  $c_1 = c_2 = 0.1$ . Note that the rate of internal relaxation is unaffected by the host properties. We also assume that the central cluster in each halo is not

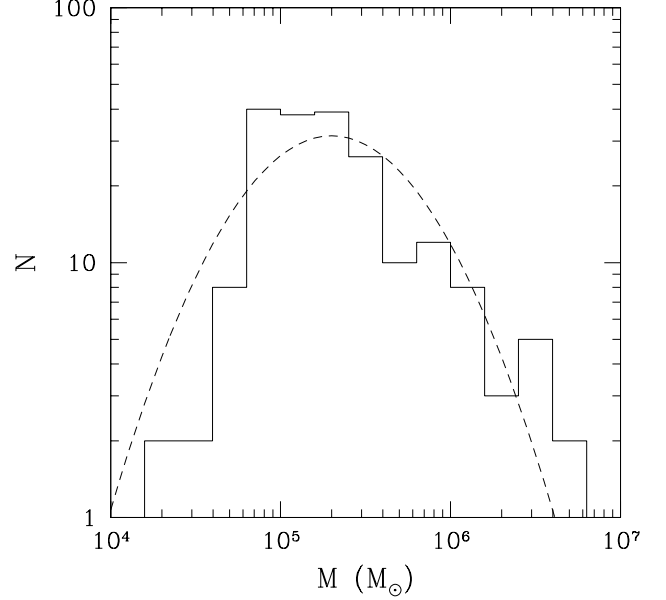


Fig. 13.1 Present-day mass function of globular clusters in our model, corrected for the effects of dynamical evolution as described in the text. Dashed line is a log-normal fit to the Galactic GCMF, normalized to have the same number of clusters as in our model. The peak and width of the log-normal function are as observed and are not fit to the model histogram.

tidally limited and therefore its evaporation time increases to  $300 t_{rh}$  (c.f., Spitzer 1987).

Figure 13 shows the evolved mass function of the model clusters at  $z = 0$ . The low-mass clusters are significantly depleted while the number of most massive clusters is only slightly affected. This results in the development of a characteristic peak at  $M \approx 10^5 M_{\odot}$ . Both the peak and the overall distribution match the observed GCMF, represented by a log-normal function, extremely well. The (25%, 50%, 75%) quartiles of the Galactic GCMF are  $\lg(M_{\text{obs}}/M) = (5.0; 5.3; 5.6)$ , while we find  $\lg(M/M) = (5.0; 5.3; 5.5)$  for the evolved mass function at  $z = 0$ .

The agreement with observations is truly remarkable, given our simple subgrid model and the approximate treatment of dynamical evolution. Although these results should be considered as preliminary, they are very encouraging. Many of the properties of cluster population arise naturally, as parameters of both the simulations and the subgrid model were not fine-tuned to reproduce them. We plan to address the issue of dynamical evolution and spatial distribution of globular clusters at  $z = 0$  in a future study, in which we will use collisionless simulations to follow the trajectories of the identified GC using a lower resolution simulation.

## 7. discussion

### 7.1. Formation of Globular Clusters at $z < 3$

In the preceding sections we analyze the formation of globular clusters at  $z > 3$ . Although the limited computational resources did not allow us to continue the simulation at the same resolution to lower redshifts, in this section we discuss the likely star cluster formation at low redshifts.

A critical question is whether we capture the formation of most of the old globular clusters at  $z > 3$  or if a significant fraction of the cluster population forms at lower redshifts.

In order to estimate the amount of star formation in all of the progenitors of the Milky Way-size galaxy at  $z < 3$ , we adapt and modify the analytical star formation model of Hernquist & Springel (2003). We substitute their unconditional mass function with the conditional mass distribution of the progenitors of a Milky Way-type halo at  $z = 0$  (Sheth & Tormen 2002), and we model the effect of reionization by including a parametrization of the filtering mass scale (Gnedin 2000). The filtering mass is defined as the mass of the halo in which the gas fraction is suppressed by a factor of two with respect to the universal value.

We find that the star formation rate for the progenitors in this model peaks at  $z = 5$ . Integrating the star formation rate over time and over the progenitor mass function, we find that 30% of the total stellar mass of the Milky Way-type galaxy is produced at  $z > 3$ . Although the majority of stars remains to be formed at  $z < 3$ , the same is not necessarily true for globular clusters. In particular, the following arguments suggest that the efficiency of globular cluster formation should be significantly reduced at lower redshifts.

First of all, the merger rate decreases rapidly as  $(1+z)^{-2.5}$  at  $z > 4$  (Gottlöber et al. 2001). It is commonly thought that galaxy mergers create conditions conducive to cluster formation. In particular, mergers stir and compress the interstellar gas creating the high-pressure environments in which dense clouds and massive stellar clusters can form. Without the mergers, star formation would likely continue in a much more quiescent mode. Figure 3 illustrates this effect. The galaxy formation simulations of Abadi et al. (2002) also show that star formation in a galaxy disk is considerably more bursty at  $z > 3$  than at lower redshifts. If mergers are connected to globular cluster formation, then a high merger rate at  $z > 3$  would lead to an almost continuous cluster formation. At lower redshifts, on the other hand, mergers become rare and most of the subsequent formation of globular clusters is likely to be limited to a single last major merger event. This picture would also naturally explain the bimodality of cluster colors observed in many elliptical galaxies.

The high-redshift disks in our simulation are small and very dense. As the disks grow in size, most of the newly accreted gas would possess larger angular momentum and would settle at larger radii in the disk. We can thus expect that the average mass-weighted density of the gas in the disk would decrease with time. In addition, the continuous star formation would consume a significant fraction of the interstellar gas, which would further decrease its density. For instance, most of the baryons in the disks in our simulation at  $z = 3.3$  are still in gaseous form, while most of the baryons in the Milky Way disk today are in stars. The lower gas density should reduce the efficiency of build-up of the highest density molecular cloud cores, thereby inhibiting the formation of massive stellar clusters (Kravtsov 2003b). The lower gas density may also make the disk more porous and more susceptible to supernova feedback, which may lead to faster dispersal of molecular clouds.

Finally, somewhat paradoxically, the globular clusters

formed at high redshifts may have a significantly higher chance of survival until the present than clusters formed at later epochs. The clusters in our model form in extremely high-density environments within the galactic disks. Strong tidal forces in such regions are likely to disrupt clusters quickly, unless they are located at the very center of the parent galaxy or are ejected from the disk by a dynamical process shortly after formation. As only a fraction of clusters form in the centers of progenitor galaxies, the latter mechanism should operate in order for the old metal-poor clusters to survive until the present.

Frequent violent mergers at high redshifts may be just such a mechanism. The mergers would disrupt the disks of the progenitor galaxies with their existing stellar populations and in part a large amount of orbital energy in the surviving clusters. The high energy orbits would allow globular clusters to spend most of the time in the relatively low-density regions of the halo, outside the main disk. At low redshifts, on the other hand, the merger rate decreases dramatically. Even if star clusters continue to form within the progenitor galaxies, they may not be able to escape the disk quickly enough to avoid disruption. This dynamical mechanism would operate both in the main disk and in all smaller mass progenitors which would eventually be accreted by the central galaxy.

This scenario implies that the formation of the globular cluster population in the inner halo of the Milky Way is closely connected to the formation of the stellar bulge and spheroid. It also implies that mergers of the progenitors would establish a spheroidal distribution of the globular cluster system, similar to that of the stellar halo, even though the clusters actually form within the disks of the progenitor systems.

The effects discussed above may result in the preferred, although extended, epoch of globular cluster formation at  $z_{GC} \approx 12$  ( $t_{GC} \approx 0.3 - 3$  G yrs for the adopted cosmological model). We see indications of this trend in our simulation. The maximum mass of the model clusters grows until  $z = 4$  and then saturates at a constant value  $\approx 4 \times 10^6 M_{\odot}$ . The total mass of the GC population forming at a given epoch also peaks around  $z = 4$  at  $\approx 2 \times 10^7 M_{\odot}$  and decreases afterward. A similar peak is observed in the total number of clusters.

We argue that the formation of globular clusters at  $z > 3$  would be associated with the increasingly rare merger events and would thus be progressively episodic. The merger rates derived from cosmological simulations (Gottlöber et al. 2001) indicate that on average galactic halos experience 1 to 4 major mergers with the mass ratio  $> 0.2$  at  $z < 2$ . Two broad evolutionary scenarios can be envisioned in this picture. If the last major merger occurs early ( $z_{merger} \approx 2$ ), not too far from the preferred epoch of GC formation, we would expect a continuous change of the cluster properties. If, on the other hand, the galaxy experiences the last major merger late ( $z_{merger} \approx 1$ ), with a substantial gap between  $z_{merger}$  and  $z_{GC}$ , the distribution of properties of the resulting cluster populations may be bimodal. The bimodality in this case would reflect a considerable change in the galactic environment (e.g., the metallicity of gas) during the interval  $z = z_{GC} - z_{merger}$ . This latter scenario is particularly relevant to the formation of large elliptical galaxies.

## 7.2. Comparison with previous work

Several recent studies explored the formation of globular clusters in the context of hierarchical cosmology using both numerical simulations and phenomenological semi-analytic models. Here we discuss and compare the specifics and results of our study to the previous simulations.

Weyl & Pudritz (2001) used Tree-SPH simulations of the CDM ( $\Omega_0 = 1$ ) cosmology to study the large-scale distribution of giant gas clouds at  $z \approx 1$  in a  $32 \text{ h}^{-1} \text{ Mpc}$  box. The authors analyzed collisions of baryonic clumps (clouds) in small-mass dark matter halos within the context of the agglomeration model of Harris & Pudritz (1994). They found a characteristic power-law spectrum of cloud masses,  $dN = dM_{\text{cloud}} / M_{\text{cloud}}^{1.7}$ , similar to the mass function of molecular clouds and young star clusters. The mass function of clouds and globular clusters in our model is consistent with this result. The detailed comparison, however, is not possible as the simulations of Weyl & Pudritz (2001) did not include star formation and the cooling of gas below  $10^4 \text{ K}$ . In addition, the low spatial resolution ( $\approx 1 \text{ kpc}$ ) prevented any detailed study of the inner structure of the clouds and as well as the density distribution and mass spectrum of clusters within individual galaxies.

Recently, Bromm & Clarke (2002) used Tree-SPH simulations to study the collapse and fragmentation of gas during the evolution of a single dwarf galaxy  $\approx 10^8 \text{ M}_\odot$  at  $z \approx 24$ . The simulation assumed that the gas was pre-enriched to the metallicity of  $10^{-2} \text{ Z}_\odot$ , which allowed the gas to cool to  $1000 \text{ K}$ , and used sink particles to follow the collapse of the gas in the highest density ( $n > 10^3 \text{ cm}^{-3}$ ) regions. The authors identified six gas clumps with masses in the range  $4 \times 10^4 \text{ to } 2 \times 10^7 \text{ M}_\odot$ , each associated with a separate small-mass dark matter halo. They concluded that the characteristic mass of globular clusters is determined by the characteristic mass of dark matter halos forming at  $z \approx 10$ .

The implicit assumption behind their conclusion is that the conditions of cluster formation exist only at the earliest stages of galaxy formation, prior to reionization. The results of our study show that, although the first globular clusters may form at  $z > 10$ , the conditions for cluster formation become more favorable at lower redshifts when more gas accumulates in the disks of the progenitor halos. Reionization does not affect significantly the formation of clusters in the relatively massive halos ( $M_h \approx 10^{10} \text{ M}_\odot$ ). Again, it is difficult to make a more detailed comparison, given the very different setup of numerical simulations and physical processes included. Yet, it is worth noting that the gas density in the most massive clump in the simulation of Bromm & Clarke (2002) (see their Fig. 3) is well below the density of dark matter. The average gas density at the resolution limit in the inner 10 pc is only  $\approx 10 \text{ M}_\odot \text{ pc}^{-3}$ , lower than the observed density of globular clusters ( $\approx 2.4$ ). The expected mass loss after cluster formation would reduce the cluster density even further. It is likely that such clumps are still insufficiently dense to form real globular clusters.

In contrast, the gas density at the sites of globular cluster formation in our simulation is considerably higher ( $\approx 100 \text{ M}_\odot \text{ pc}^{-3}$ ) and is typically at least an order of magnitude higher than the local density of dark matter. We

further assume that the clusters form only at densities  $> 10^4 \text{ M}_\odot \text{ pc}^{-3}$  within the collapsing isothermal molecular cores. The fact that GC formation sites are strongly baryon-dominated explains the absence of dark matter halos around globular clusters. Bromm & Clarke (2002), on the other hand, conjecture that dark matter hosts of globular clusters dissolve via violent relaxation before the cluster forms, while the baryonic core survives.

Both of the above studies attribute the shape of the GC mass function to the distribution of their parent dark matter halos. Our results indicate that the situation is more complex. We have shown that the shape of the GCMF is determined both by the mass function of the parent halos and the mass distribution of clusters within a single halo ( $\approx 4$ ).

Bearley et al. (2002) extended the semi-analytical model of galaxy formation GALFORM to include a phenomenological prescription of GC formation. The model assumed that a constant fraction of stellar mass,  $\eta$ , would be in the form of globular clusters. The blue (metal-poor) clusters were associated with the quiescent mode of star formation, while the red (metal-rich) clusters were assumed to form during starbursts. The parameters,  $\eta = 0.002$  for blue clusters and  $\eta = 0.007$  for red clusters were set to agree with the observed color distribution of the elliptical galaxy NGC 4472. However, Bearley et al. (2002) truncated the formation of blue clusters arbitrarily at  $z = 5$  to create a distinctly bimodal distribution of colors in their model. In addition they find an age-metallicity correlation for their model clusters, which is a definite prediction of semi-analytical models. In contrast, our simulation follows the gas dynamics and metal enrichment self-consistently and does not predict any clear age-metallicity relation.

## 8. Summary

We have presented a study of globular cluster formation at  $z > 3$  using a very high-resolution cosmological simulation. The clusters in our model form in the high-density isothermal cores of giant molecular clouds in dense gas disks of high-redshift galaxies. The properties of globular clusters are estimated using a simple physically-motivated subgrid model. Many of the observed properties of globular clusters are reproduced naturally, i.e., without tuning. Our main conclusions can be summarized as follows.

The first globular clusters in the Galaxy formed around  $z \approx 12$  and cluster formation continued at least until  $z \approx 3$ . We argue ( $\approx 7.1$ ) that the overall efficiency of globular cluster formation is significantly reduced at lower redshifts with most clusters at  $z \approx 2$  forming in rare gas-rich galactic mergers. The preferred epoch of globular cluster formation is  $z \approx 3.5$  (or  $\approx 1.2 \text{ Gyr}$  in the adopted cosmology) when the gas supply is abundant in the disks of the progenitor halos and the merger rate of the progenitors is high. All old globular clusters thus appear to have similar ages.

Most globular clusters in our model form in halos of mass  $\approx 10^9 \text{ M}_\odot$ . The spatial distribution of these halos at  $z > 3$  is highly clustered (biased) with respect to the overall distribution of matter ( $\approx 3.1$ ).

The high spatial bias of their parent halos explains the present more concentrated radial distribution of globular clusters relative to dark matter. Within the progenitor systems, globular clusters form in the highest-density regions of the disk. In the most massive disk in the simulation, the newly formed clusters trace the spiral arms and the nucleus similarly to the young stellar clusters observed in merging and starbursting galaxies. Subsequent mergers of the progenitor galaxies lead to the overall spherical distribution of clusters at present (§ 7.1).

The mass function of globular clusters at birth can be approximated by a power-law  $dN/dM \propto M^{-1.5 \pm 2}$ , in good agreement with observations of young star clusters in interacting galaxies. The shape of the mass function is determined both by the mass function of parent galaxies and the mass distribution of molecular cloud cores within each halo. Although the physical processes governing the evolution of the halos and molecular clouds are completely different, their mass distributions can both be approximated by the power-law functions with  $-1.5 \pm 2$ .

The halo mass function arises during the hierarchical build-up of structures in the expanding universe from the initial random perturbations. The mass function of the molecular clouds cores, on the other hand, samples the underlying log-normal density probability distribution function (PDF) of the gas in the galactic disks. The log-normal shape of the high-density tail of the PDF, in turn, is due to the supersonic turbulence driven by mergers and shearing instabilities in the nearly isothermal gas.

The zero-age mass function of globular clusters in our model has the same shape as the mass function of their parent molecular cloud cores. The model therefore predicts that the true shape of the cluster mass function is log-normal (eq. 11) but with a peak at very low masses,  $\sim 10^3 M_{\odot}$ . Over the range of masses typically probed in observations,  $M \gtrsim 10^5 M_{\odot}$ , the mass function can be approximated by a power-law because the expected curvature over this range is rather small. Nevertheless, we find that the steepening of the logarithmic slope of the mass function may be detectable.

The dynamical evolution of globular clusters until the present would preferentially deplete the low-mass end of the distribution. We apply a simple dynamical evolution model to our zero-age mass function and find an excellent agreement with the observed mass function of the Galactic globular clusters.

The distribution of sizes and metallicities of the massive ( $M > 10^5 M_{\odot}$ ) globular clusters match those of the Galactic globulars, with the exception of the largest size and the highest metallicity tail. It is plausible that these discrepancies can be rectified by dynamical evolution and the continuing formation of globular clusters at  $z < 3$ .

The local efficiency of globular cluster formation within the parent molecular cloud is  $M_{\text{GC}}/M_{\text{cloud}} \sim 10^{-3}$ , with considerable scatter. The global efficiency, the ratio of the total globular cluster mass to the baryonic mass of the parent galaxy, is  $M_{\text{GC}}/M_{\text{b}} \sim (2-3) \times 10^{-4}$ . The mass in globular clusters scales with the total galaxy mass as  $M_{\text{GC}} \propto M_{\text{h}}^{1.1}$  (eq. [6]). These values for the formation efficiencies are in general agreement with observations (Harris & Pudritz 1994; McLaughlin 1999).

We find that the mass of the globular cluster population and the maximum cluster mass in a given region strongly correlate with the local average star formation rate density:  $M_{\text{max}} \propto (\text{SFR})^{0.54 \pm 0.07}$  and  $M_{\text{GC}} \propto (\text{SFR})^{0.75 \pm 0.06}$  at  $z = 3.3$ . A similar correlation exists for the observed present-day galaxies (Larsen 2002). The correlation arises because both the star formation rate and mass of the globular cluster population are controlled by the amount of gas in the densest regions of the ISM.

Our model predicts the lack of clear age-metallicity and mass-metallicity correlations, at least for the clusters with  $[\text{Fe}/\text{H}] < -1$ . Although there is an overall trend of increasing the average metallicity with time, a significant spread of metallicities exists among different progenitor galaxies and within the interstellar medium of each galaxy. The old stars and stellar clusters forming at a given epoch in simulation exhibit scatter in metallicity of up to two orders of magnitude.

In future work, we plan to study the details of the dynamical evolution of the globular cluster population by extending our current simulation to  $z = 0$ . We will incorporate our subgrid model of star cluster formation directly in the high-resolution simulations of galaxy formation. We will also test alternative subgrid models to investigate the effects of different formation criteria on the observable properties of globular cluster populations.

Our present results are encouraging and demonstrate that globular clusters with properties similar to the observed clusters form naturally within young  $z \approx 3$  galaxy disks in the standard CDM cosmology. The optimal conditions for cluster formation appear to be at  $z \approx 5$ , coinciding with the peak of global star formation rate. As the formation of first stars marks the end of the cosmic dark ages (Rees 1997), the formation of globular clusters thus marks a veritable stellar renaissance of the Universe.

We would like to thank M. Fall, D. Lamb, G. Meylan, and J. Truran for stimulating discussions on globular cluster formation, and Q. Zhang for providing the mass function for the Antennae. The simulations and analyses presented here were performed on the IBM RS/6000 SP system at the National Energy Research Scientific Computing Center (NERSC) and on the Origin2000 at the National Center for Supercomputing Applications (NCSA). This work was supported by the National Science Foundation under grants No. AST-0206216 and AST-0239759 (CAREER) to the University of Chicago. OYG is supported by the STScI Fellowship.

## REFERENCES

Abadi, M. G., Navarro, J. F., Steinmetz, M., & Eke, V. R. 2002, *astro-ph/0212282*

Anders, E. & Grévesse, N. 1989, *Geochim. Cosmochim. Acta*, 53, 197

Ashman, K. M. & Zepf, S. E. 1992, *ApJ*, 384, 50  
| . 2001, *AJ*, 122, 1888

Bate, M. R., Bonnell, I. A., & Bromm, V. 2003, *MNRAS*, 339, 577

Beasley, M. A., Baugh, C. M., Forbes, D. A., Sharples, R. M., & Frenk, C. S. 2002, *MNRAS*, 333, 383

Bromm, V. & Clarke, C. J. 2002, *ApJ*, 566, L1

Burkert, A., Tsuran, J. W., & Hensler, G. 1992, *ApJ*, 391, 651

Côte, P., Marzke, R. O., West, M. J., & Minniti, D. 2000, *ApJ*, 533, 869

Côte, P., West, M. J., & Marzke, R. O. 2002, *ApJ*, 567, 853

Carney, B. W. 1996, *PA SP*, 108, 900

Carney, B. W. 2001, in *Star Clusters, Saas-Fee Advanced Course 28. Lecture Notes 1998*, Swiss Society for Astrophysics and Astronomy. Edited by L. Labhardt and B. Binggeli (Springer-Verlag Berlin), 1{222

Caron, R. 2001, *ApJ*, 560, 592

Chen, D. F. & Weinberg, M. D. 1990, *ApJ*, 351, 121

Cohen, J. G., Blakeslee, J. P., & Côte, P. 2003, *astro-ph/0304333*

Cohen, J. G., Blakeslee, J. P., & Ryzhov, A. 1998, *ApJ*, 496, 808

Colella, P., & Glaž, H. M. 1985, *J. Comp. Phys.*, 59, 264

Colpi, M., Mayer, L., & Governato, F. 1999, *ApJ*, 525, 720

Dekel, A. & Woo, J. 2003, *MNRAS*, submitted *astro-ph/0210454*

Djorgovski, S. & Meylan, G. 1994, *AJ*, 108, 1292

Elmegreen, B. G. 2002, *ApJ*, 577, 206

Elmegreen, B. G. & Elmehov, Y. N. 1997, *ApJ*, 480, 235

Elson, R. A. W. & Fall, S. M. 1985, *PA SP*, 97, 692

Fall, S. M. & Rees, M. J. 1985, *ApJ*, 298, 18

Fall, S. M. & Zhang, Q. 2001, *ApJ*, 561, 751

Ferland, G. J., Korista, K. T., Verner, D. A., Ferguson, J. W., Kingdon, J. B., & Verner, E. M. 1998, *PA SP*, 110, 761

Geyer, M. P. & Burkert, A. 2001, *MNRAS*, 323, 988

Gnedin, N. Y. 2000, *ApJ*, 542, 535

Gnedin, O. Y. 2003, in *Extragalactic Globular Cluster Systems*, ed. M. K. Kissler-Patig (Springer), *astro-ph/0210556*

Gnedin, O. Y., Lahav, O., & Rees, M. J. 2001, *astro-ph/0108034*

Gnedin, O. Y., Lee, H. M., & Ostriker, J. P. 1999, *ApJ*, 522, 935

Gnedin, O. Y. & Ostriker, J. P. 1997, *ApJ*, 474, 223

Gottlöber, S., Klypin, A., & Klytsov, A. V. 2001, *ApJ*, 546, 223

Gunn, J. E. 1980, in *Globular Clusters*, D. Hanes and B. Madore eds., (Cambridge Univ. Press), 301

Harris, W. E. 1996, *AJ*, 112, 1487

Harris, W. E. 2001, in *Star Clusters, Saas-Fee Advanced Course 28. Lecture Notes 1998*, Swiss Society for Astrophysics and Astronomy. Edited by L. Labhardt and B. Binggeli (Springer-Verlag Berlin), 223{408

Harris, W. E. & Pudritz, R. E. 1994, *ApJ*, 429, 177

Hemquist, L. & Springel, V. 2003, *MNRAS*, submitted, *astro-ph/0209183*

Holtzman, J. A., Watson, A. M., Mould, J. R., Gallagher, J. S., Ballester, G. E., Burrows, C. J., Clarke, J. T., Crisp, D., Evans, R. W., Griffiths, R. E., Hester, J. J., Hoessel, J. G., Scowen, P. A., Stapelfeldt, K. R., Trauger, J. T., & Westphal, J. A. 1996, *AJ*, 112, 416

Hu, W. & Sugiyama, N. 1996, *ApJ*, 471, 542

Jungwiert, B., Combes, F., & Palous, J. 2001, *A & A*, 376, 85

Khokhlov, A. M. 1998, *J. Comp. Phys.*, 143, 519

Klypin, A., Klytsov, A. V., Bullock, J. S., & Primack, J. R. 2001, *ApJ*, 554, 903

Klypin, A., Zhao, H., & Somerville, R. S. 2002, *ApJ*, 573, 597

Komendy, J. 1985, *ApJ*, 295, 73

Klytsov, A. V. 1999, PhD thesis, New Mexico State University | . 2003a, *ApJ*, in preparation | . 2003b, *ApJL* in press, *astro-ph/0303240*

Klytsov, A. V., Klypin, A. A., & Khokhlov, A. M. 1997, *ApJS*, 111, 73

Kroupa, P., Arseth, S., & Hurley, J. 2001, *MNRAS*, 321, 699

Larsen, S. S. 2002, *AJ*, 124, 1393

Larson, R. B. 1981, *MNRAS*, 194, 809

Larson, R. B. 1996, in *ASP Conf. Ser. 92: Formation of the Galactic Halo...Inside and Out*, 241

Lee, J. & Carney, B. W. 2002, *AJ*, 124, 1511

McLaughlin, D. E. 1994, *PA SP*, 106, 47 | . 1999, *AJ*, 117, 2398

McLaughlin, D. E. & Pudritz, R. E. 1996, *ApJ*, 457, 578

Meurer, G. R., Heckman, T. M., Leitherer, C., Kinney, A., Robert, C., & Gamett, D. R. 1995, *AJ*, 110, 2665

Miller, G. E. & Scalo, J. M. 1979, *ApJS*, 41, 513

Moore, B. 1996, *ApJ*, 461, L13

Murali, C. & Weinberg, M. D. 1997, *MNRAS*, 288, 749

Murray, S. D. & Lin, D. N. C. 1992, *ApJ*, 400, 265

Nakasato, N., Mori, M., & Nomoto, K. 2000, *ApJ*, 535, 776

Ostriker, E. C., Stone, J. M., & Gammie, C. F. 2001, *ApJ*, 546, 980

Padmanabhan, P., Jimenez, R., & Jones, B. 1997, *MNRAS*, 285, 711

Peebles, P. J. E. 1984, *ApJ*, 277, 470

Peebles, P. J. E. & Dicke, R. H. 1968, *ApJ*, 154, 891

Press, W. H. & Schechter, P. 1974, *ApJ*, 187, 425

Pringle, J. E. 1989, *MNRAS*, 239, 361

Rees, M. J. 1997, Before the beginning. Our universe and others (Reading: Addison-Wesley)

Scalo, J., Vazquez-Semadeni, E., Chappell, D., & Passot, T. 1998, *ApJ*, 504, 835

Schweizer, F. 1987, in *Early Normal Galaxies. From the Planck Time to the Present*, 18{25

Shapley, H. 1930, *Star Clusters (McGraw-Hill: New York)*, 193

Sheth, R. K. & Tormen, G. 1999, *MNRAS*, 308, 119 | . 2002, *MNRAS*, 329, 61

Smith, G. H., Sneden, C., & Kraft, R. P. 2002, *AJ*, 123, 1502

Solomon, P. M., Rivolo, A. R., Barrett, J., & Yahil, A. 1987, *ApJ*, 319, 730

Spergel, D. N., Verde, L., Peiris, H. V., Komatsu, E., Nolta, M. R., Bennett, C. L., Halpern, M., Hinshaw, G., Jarosik, N., Kogut, A., Limon, M., Meyer, S. S., Page, L., Tucker, G. S., Weiland, J. L., Wollack, E., & Wright, E. L. 2003, *ApJ* submitted, *astro-ph/0302209*

Spitzer, L. 1987, *Dynamical Evolution of Globular Clusters* (Princeton: Princeton University Press)

Vazquez-Semadeni, E., Gázola, A., & Scalo, J. 2000, *ApJ*, 540, 271

van den Bergh, S. 1996, *AJ*, 112, 2634 | . 2003, *astro-ph/0303042*, 3042

van Leer, B. 1979, *J. Comp. Phys.*, 32, 101

Vazquez-Semadeni, E. 1994, *ApJ*, 423, 681

Vesperini, E. 1998, *MNRAS*, 299, 1019

Vesperini, E. & Heggie, D. C. 1997, *MNRAS*, 289, 898

Wada, K. & Nomura, C. A. 2001, *ApJ*, 547, 172

Weil, M. L. & Pudritz, R. E. 2001, *ApJ*, 556, 164

West, M. J. 1993, *MNRAS*, 265, 755

Whitmore, B. C. 2000, *astro-ph/0012546*

Whitmore, B. C. & Schweizer, F. 1995, *AJ*, 109, 960

Whitmore, B. C., Zhang, Q., Leitherer, C., Fall, S. M., Schweizer, F., & Miller, B. W. 1999, *AJ*, 118, 1551

Wong, T. & Blitz, L. 2002, *ApJ*, 569, 157

Woozley, S. E. & Weaver, T. A. 1995, *ApJS*, 101, 181

Young, J. S., Allen, L., Kenney, J. D. P., Lesser, A., & Rownd, B. 1996, *AJ*, 112, 1903

Zepf, S. E., Ashman, K. M., English, J., Freeman, K. C., & Sharples, R. M. 1999, *AJ*, 118, 752

Zhang, Q. & Fall, S. M. 1999, *ApJ*, 527, L81

Zhang, Q., Fall, S. M., & Whitmore, B. C. 2001, *ApJ*, 561, 727